Final Report 2009 - 2012
Hall MHD Stability and Turbulence in Magnetically Accelerated Plasmas
DE-SC0001049

H.R. Strauss
HRS Fusion

Executive Summary

This is a summary of research work performed on "Hall MHD Stability and Turbulence in Magnetically Accelerated Plasmas," DE-SC0001049. The object of the research was to develop theory and carry out simulations of the Z pinch and plasma opening switch (POS), and compare with experimental results. In the case of the Z pinch, there was experimental evidence of ion kinetic energy greatly in excess of the ion thermal energy [1, 2]. It was thought that this was perhaps due to fine scale turbulence. The simulations showed that the ion energy was predominantly laminar, not turbulent [3]. Preliminary studies of a new Z pinch experiment with an axial magnetic field were carried out. The axial magnetic is relevant to magneto - inertial fusion [4]. These studies indicate [5] the axial magnetic field makes the Z pinch more turbulent. Results were also obtained on Hall magnetohydrodynamic instability of the POS.

2D Z pinch simulations

A part of the proposal was to study turbulence in Z pinches and compare with experimental results, in particular the WIS low density gas puff Z pinch [1, 2]. It was thought that this and other experiments detect anomalous turbulent ion kinetic energy during the stagnation of the Z pinch [6].

Two dimensional simulations were done with a modified version of the M3D extended MHD code [7], which uses a 2D unstructured mesh to obtain high resolution in both radial and axial directions at the cylindrical axis. A radiation model was added, which appeared adequate to model the features of the experiment and to assess the turbulence during the stagnation of the Z pinch.

In particular, some features of the experiment were

(1) the stagnated plasma column expands and then shrinks,

(2) ion kinetic energy during stagnation is greatly in excess of the electron thermal energy. The ion kinetic energy is measured as a line broadening spectroscopically, but it cannot be a temperature. The high collision frequency ensures that ions and electrons have close to the same temperature of several hundred eV. The anomalous "effective ion temperature" is almost 10 times higher, and it decays on the timescale of the stagnation [1]. It was attributed to turbulence;

(3) images in visible light showed large scale axially symmetric perturbation structures outside the column, and later evidence of MHD instability of the column.

Experimental observation (1) is explained by the M3D simulations as follows:

The simulations showed that during implosion, a shock is driven by the magnetic piston [8]. The piston front is Rayleigh Taylor unstable, but the shock front, traveling ahead of the

piston, is stable. The shock reaches the axis and reflects, starting the stagnation phase. The high density core expands, until it collides with the incoming magnetic piston. This causes the core to shrink again.

Observation (2) is explained by the reflection of the shock front, collision with the magnetic piston, and the setting up of a quasi equilibrium state. The core is not turbulent, until the expanding shock collides with the incoming Rayleigh Taylor unstable magnetic piston. Instead the ion energy is directed, largely laminar motion. It was observed as line broadening, rather than as a Doppler shift, due to the experimental arrangement. The radiation from the stagnated core was integrated along a chord passing nearly through the geometric origin; hence a radial flow gives nearly equal positive and negative Doppler shifts which evidently appeared as line broadening. Unfortunately it is almost impossible to change the experimental line of sight. The ion kinetic energy can be found by by balancing ion kinetic energy with pressure in the stagnated core. While the electron and ion temperatures are nearly equal, the electron density is Z times larger than the ion density, where $Z \approx 6$ is the effective ion charge. This gives a ratio of kinetic energy per ion mass density to temperature of about $(Z + 1)$, which accounts for the large ratio of effective ion temperature to electron temperature. Much of the ion kinetic energy is radiated away. It is comparable to the magnetic energy density at the piston.

Observation (3) of the large scale MHD instability is explained by the Rayleigh Taylor instability of the magnetic piston.

These findings have been published in H. Strauss, Stagnation of a gas puff Z pinch, Phys. Plasmas **19**, 032705 (2012).

A reprint is attached as an Appendix.

POS simulations

Hall turbulence and shock propagation in POS

A preliminary study of Hall MHD turbulence in a POS was carried out. The study showed the excitation of turbulence at the plasma boundary. The study also showed the the penetration of magnetic field into the POS was insensitive to magnetic polarity. This study is attached as Appendix B.

current channel width in POS

Simulational studies of a plasma opening switch (POS) [9] were carried out. The POS is interesting because it is in the Hall MHD regime. Previous theory has been reasonably successful in explaining features of POS experiments [9]. Several experimental features have been unexplained, in particular the following:

(1) The current channel width is much wider than predicted. It is measured to be much wider than a resistive diffusion scale or skin depth.

(2) Different ion species show different dynamics. The plasma consists of protons and carbon ions. The protons move ahead of the magnetic field front, while the heavy ions are penetrated by the magnetic field and lag behind the magnetic field front.

(3) The evolution of a broad ion velocity distribution was observed [10].

The two features (1) and (2) can be explained by including finite temperature in the dynamics, which was neglected in previous theory. Feature (3) is evidently caused by Hall

MHD turbulence. Simulations, in progress, with the M3D code confirm these features.

A preprint of this work is attached as Appendix c.

3D Z pinch simulations

A new experiment at Weizmann Institute of Science (WIS) with an applied axial magnetic field has recently been constructed and is beginning to operate. The experiment will employ spectroscopic techniques to obtain magnetic field data, measurements of kinetic energy, density, and temperature. The additional axial field is motivated by the present interest in magneto inertial fusion, in particular magnetized liner inertial fusion (MagLIF) [4]. The addition of an axial field also permits the development of new instabilities, including g modes (localized Rayleigh Taylor instabilities) and current driven instabilities, not usually studied in the context of Z pinches. The axial magnetic field makes the Z pinch into a type of screw pinch, and it becomes subject to instabilities typical of tokamaks, stellarators, and other devices containing a sheared magnetic field.

Some preliminary theory and 3D simulations relevant to the WIS experiment have been carried out. They were presented at the ICOPS conference, Edinburgh, 2012, and summarized in the following. The results demonstrate the expected stabilization of the magnetized Rayleigh Taylor instability at the magnetic piston interface. They also show development of magnetic turbulence outside the magnetic piston interface, in the region of sheared magnetic field. Preliminary analysis identified the turbulent region with the region of kink mode instability.

The following preliminary simulations were performed with the M3D code, which is described below. The simulations were three dimensional. An initial state similar to those of [3], except that an initially spatially constant axial magnetic field is included. The plasma was allowed compress and stagnate. Two cases are compared. In Fig.1, the initial axial field is small, $B_z^0 = 0.02 B_\theta^0$. Shown in Fig.1(a) is $B_\theta(r, z, 0)$ at stagnation. The perturbations of $B_\theta(r, z, 0)$ is similar to those produced by Rayleigh Taylor instability in [3]. A slice of $B_\theta(r, L/2, \theta)$ and is shown in Fig.2(a) of the same case at the same time, showing that the perturbations are predominantly $m = 0$, with an $m = 1$ component. In Fig.1(b) and Fig.2(b) are shown as case with larger $B_z^0 = 0.10 B_\theta^0$. The magnetic field is quite different from Fig.1(a), Fig.2(a). The perturbations are replaced by shorter wavelength modes, localized outside the stagnation region.

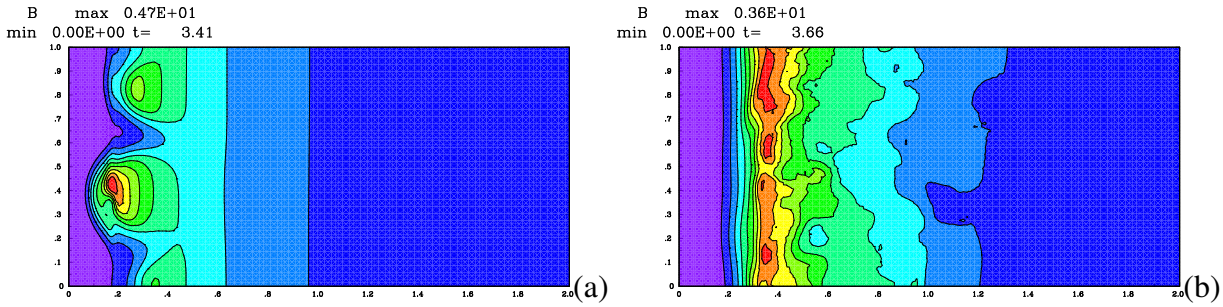

(a) (b)

Figure 1: (a) The magnetic azimuthal field B_θ in $(r, z, 0)$ plane, at time $t = 3.41\tau_A$, at stagnation. The axial field is 0.02 the initial azimuthal field. The perturbations are produced by Rayleigh Taylor instability. (b) The field B_θ in $(r, z, 0)$ plane, at time $t = 3.66\tau_A$, at stagnation, where the initial axial field is 0.10 the initial azimuthal field. In the low axial field case, the perturbations reach the axis, while in the high axial field case, the perturbations are of a different appearance, and occur in the region outside the stagnated core, with high k_z.

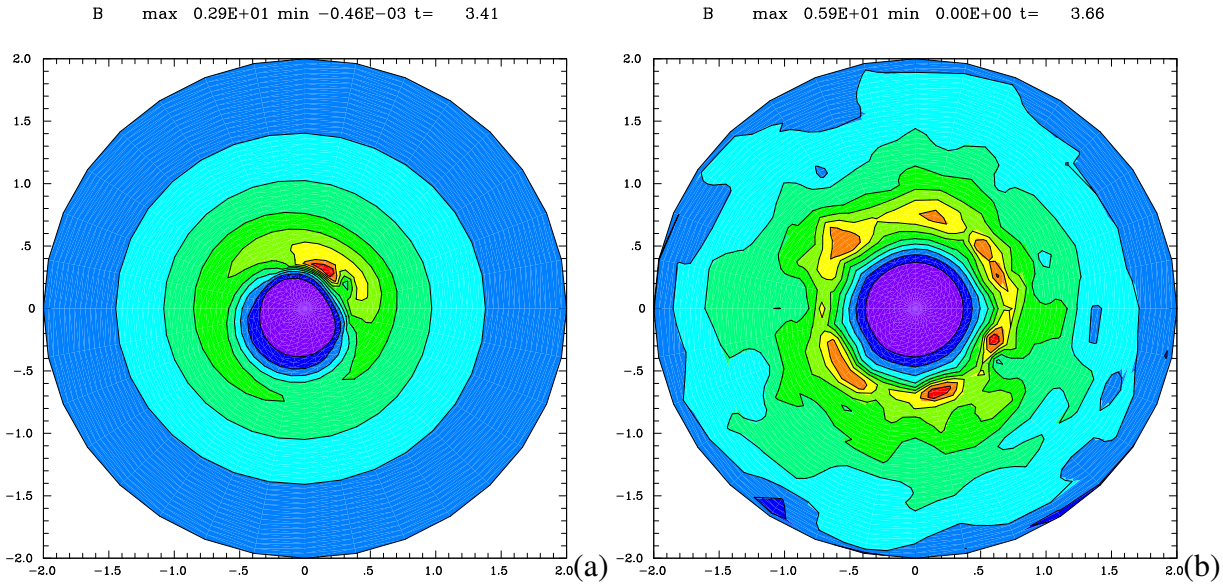

(a) (b)

Figure 2: The azimuthal field B_θ at the same times as in the previous figure except that the $(r, L/2, \theta)$ plane is shown. (a) As in Fig.1(a), showing predominantly $m =$ structure with some $m = 1$. (b) As in Fig.1(b), showing high m structure. Theoretically the perturbations have helical structure, with $\mathbf{B} \cdot \mathbf{k} \approx 0$.

The ICOPS presentation is given as Appendix D.

Meetings and Laboratory Visits

Attended and made presentations at APS meeting Z pinch session, 2009,2010,2011. Attended and gave talk at ICOPS meeting Z pinch session, 2012.

Several visits to WIS laboratory, 2009,2010,2011,2012.

Visited Imperial College London, Physics Department, Plasma Physics Z Pinch Laboratory, March 2010.

References

[1] E. Kroupp, D. Osin, A. Starobinets, V. Fisher, V. Bernshtam, Y. Maron, I. Uschmann, E. Forster, A. Fisher, and C. Deeney, Ion - kinetic - energy measurements and energy balance in a z - pinch plasma at stagnation, Phys. Rev. Lett. **98** 115001 (2007).

[2] E. Kroupp, D. Osin, A. Starobinets, V. Fisher, V. Bernshtam, L. Weingarten, Y. Maron, L. Uschmann, E. Förster, A. Fisher, M. E. Cuneo, C. Deeney, and J. L. Giuliani, Ion temperature and hydrodynamic - energy measurements in a z - pinch plasma at stagnation, *submitted to Phys. Rev. Lett.*, 2011.

[3] H. Strauss, Stagnation of a gas puff Z pinch, Phys. Plasmas **19**, 032705 (2012).

[4] S. A. Slutz, M. C. Herrmann, R. A. Vesey, A. B. Sefkow, D. B. Sinars, D. C. Rovang, K. J. Peterson, and M. E. Cuneo, Phys. Plasmas **17**, 056303 (2010).

[5] H. Strauss, Stagnation of a gas puff Z pinch, paper 1P-169 ICOPS meeting, Edinburg, July 8-12 (2012).

[6] M. G. Haines, P. D. LePell, C. A. Coverdale, B. Jones, C. Deeney, and J. P. Apruzese Phys. Rev. Letters **96**, 075003 (2006).

[7] W. Park, E.V. Belova, G.Y. Fu, X. Tang, H.R. Strauss, L.E. Sugiyama, Plasma Simulation Studies using Multilevel Physics Models, Phys. Plasmas **6**, (1999) 1796.

[8] D. D. Ryutov, M. S. Derzon, M. K. Matzen, The physics of fast Z pinches, Rev. Mod. Phys. **72**, 167 (2000).

[9] H.R. Strauss, R. Doron, R. Arad, B. Rubinstein, Y. Maron, A. Fruchtman, Magnetic field propagation in a two ion species planar plasma opening switch, Physics of Plasmas **14** 053504 (2007).

[10] R. Doron, R. Arad, K. Tsigutkin, A. Weingarten, A. Starobinets, V. A. Bernshtam, E. Stambulchik, Yu. V. Ralchenko, Y. Maron, A. Fructman, A. Fisher, J. D. Huba, M. Roth Plasma dynamics in pulsed strong magnetic fields, Phys. Plasmas, **11**, 2411 (2004).

Stagnation of a gas puff Z pinch

H. R. Strauss[a)]
HRS Fusion, West Orange, New Jersey 07052, USA

(Received 26 September 2011; accepted 12 March 2012; published online 30 March 2012)

Simulations of a gas puff Z pinch were performed, using an appropriately modified version of the M3D code [Park *et al.*, Phys. Plasmas **6**, 1796 (1999)]. The simulations investigated the stagnation process, including the effects of the shock driven by the magnetic piston and the influence of the Rayleigh Taylor instability. The results compare favorably with recent experimental measurements. The stagnated plasma reaches a quasi equilibrium with approximate balance of plasma pressure and magnetic pressure, measured by $\beta \leq 1$. The dependence of the stagnation radius on β and radiative energy loss are calculated, using a simple radiation model. © *2012 American Institute of Physics*. [http://dx.doi.org/10.1063/1.3697979]

I. INTRODUCTION

The Z pinch is a candidate as a driver for inertial fusion, either in its own right or in related magneto-inertial approaches.[1–4] In a gas puff Z pinch, an intense axial current is made to flow in a cylindrical plasma shell. The radially inward Lorentz force implodes the shell of plasma toward the axis of the cylinder. When the plasma reaches the axis, the inflow stagnates. The plasma is compressed to high density and temperature. A problem with the Z pinch, as with other accelerating plasmas, is the Rayleigh Taylor instability. This can cause the imploding plasma to fragment during stagnation. The present paper is motivated by recently reported studies of stagnation in a neon gas puff Z pinch.[5,6] In the experiment, the ion kinetic energy was measured directly from spectroscopic data, and shown to be mostly in hydrodynamic motion, rather than in thermal energy. During the stagnation time $t_s = 10$ ns, the ion kinetic energy decayed to about 10% of its value at the beginning of stagnation. During stagnation, the plasma was measured to have electron density $n_e = 6 \pm 3 \times 10^{20}\,\mathrm{cm}^{-3}$, electron temperature $T_e \approx 200\,\mathrm{eV}$, and average ion charge $Z = 8$–9.5. The peak applied current was 500 KA. The stagnation radius r_s was about 0.5 mm. The Alfvén speed was $v_A \approx 1.2 \times 10^7\,\mathrm{cm/s}$. This is consistent with a stagnation time $t_s \approx 2.4 r_s/v_A = 10\,\mathrm{ns}$.

Under these conditions,[7] the electron-ion temperature equilibration time is about $0.1\mathrm{ns} \ll t_s$. Hence, the ion temperature T_i was nearly the same as the electron temperature T_e during stagnation. The ion-ion collision time was $\tau_{ii} \approx 2.3 \times 10^{-13}$ s, which is much shorter than the stagnation time t_s. During implosion, it was also the case that τ_{ii} was short compared to the timescale of the motion r/v_A, the radius of the plasma divided by the Alfvén speed. If it is assumed that T_i, n_i, B varied adiabatically during implosion (see Sec. III), then the ratio of the ion-ion collision time to the implosion timescale, $\tau_{ii} v_A/r \approx 0.36 \times (1/Z)^4 r_s/r$. This was less than unity during the implosion, even for $Z = \mathcal{O}(1)$. Hence, it could not be the case that the plasma had low collisionality during implosion and then thermalized in an ion-ion collision time at stagnation.[3,6] The collisionality was sufficiently high that the plasma was well described by magnetohydrodynamics (MHD) during implosion and stagnation.

In the experiment, the ion kinetic energy was measured in the beginning of stagnation to be about 10 times the ion pressure. The paper[6] cautiously states that "the nature of the hydrodynamic motion that dominates the ion kinetic energy at stagnation is not clear as yet." It was thought that perhaps the motion was turbulent.[8] The present paper shows that the ion energy is not primarily due to turbulence but produced by the laminar inflow of the implosion. It is noteworthy that in other Z pinch experiments, the ion kinetic energy is apparently much higher than the implosion kinetic energy.[9–11] In those experiments the ion-electron temperature equilibration time is relatively long compared to the stagnation time, so the ion temperature can greatly exceed the electron temperature. There the high ion temperature may be caused by viscous heating caused by dissipation of g mode turbulence.[12] In the experiment considered here, the ion-electron temperature equilibration time is short compared to the stagnation time, so that ion and electron temperatures were nearly equal. Representative values of Reynolds number during implosion were $R_e \approx 10^6$ in the unmagnetized region and $R_e \approx 10^3$ in the magnetized region. The magnetic Lunquist number was $S \approx 10^4$. These values are such that viscous and resistive heating are not very important.

The simulations and theory presented here offer an explanation of the effective ion energy. It is laminar kinetic energy due to the implosion of the plasma. The ion kinetic energy in the stagnation region is comparable to the pressure. This gives a scaling of the ratio of kinetic energy per ion to temperature proportional to $Z + 1$, which in this case is about 10. There is a turbulent component of the kinetic energy in the stagnation region, but it is not important in the initial stage of the stagnation process.

It is shown that the radius of the high density plasma core in stagnation expands from zero and then contracts, similar to experimental observation.[5,6] The maximum stagnation radius r_s depends on the ratio of plasma pressure in the core to magnetic pressure outside the core, measured by the quantity $\beta \leq 1$, defined below. The effect of radiative

a)Electronic mail: hankrs2@gmail.com.

energy loss on the stagnation radius is calculated, using a simple radiation model. Radiation produces a smaller stagnation radius.

According to the simulations presented here, the ion motion in the core, in the beginning of the stagnation phase, is not turbulent. Turbulence is introduced to the stagnation region by collision of the expanding core with the incoming Rayleigh Taylor unstable magnetic piston.

Visible light visualization of the imploding Z pinch reveal larger scale features as well,[13] which resemble nonlinear Rayleigh Taylor instability.

The stagnation of the simulated gas puff Z pinch begins with a shock wave[3] reaching the axis and reflecting. The shock wave is produced during implosion. The magnetic piston pushes on the plasma, compressing it. The temperature of the compressed plasma gives the plasma piling up on the piston front a high pressure. This causes the plasma to expand ahead of the piston, creating a shock wave. During the implosion, there is a region of moderately high density unmagnetized plasma between the shock and the piston. This region is bounded by the shock front radius and the magnetic piston. The shock front is evidently stable, unlike the piston-plasma interface, which is unstable.

The stagnation phase begins when the shock front reaches the axis. The high density plasma column reflects from the axis and expands. At this point, the stagnated plasma is unmagnetized and is not turbulent. Shortly after, the magnetic piston arrives and hits the outgoing reflected shock. This causes the plasma column to shrink in diameter and transfers turbulent motion from the piston front to the stagnated column. The timescale for the expansion and contraction phase of stagnation is comparable to a sound or Alfvén wave transit time across the column, consistent with experimental observations.

The expansion and contraction of the stagnated plasma is observed experimentally. The radiating plasma region is seen to expand and contract in x ray pinhole images.[5,6]

The ion kinetic energy in the stagnated column is predominantly laminar motion of the shock, first reflecting from the axis and then from the incoming piston. The experimental observations[5,6] could not distinguish laminar from turbulent motion. Radiation emitted by the plasma was integrated along a chord passing nearly through the geometric axis. This sampled Doppler shifts corresponding to a range of velocities along the line of sight, including zero velocity. The standard deviation of the Doppler shifts was interpreted as a temperature-like effective energy. This did not give information about the radial structure of the plasma velocity.

The measurements indicated that the effective ion temperature obtained from spectral broadening was about an order of magnitude greater than the electron temperature. In turn, the ion and electron temperatures should be nearly equal because the collisional equilibration time is much shorter than the stagnation time at the measured ion density. It was concluded that the effective ion temperature was produced by hydrodynamic motion.[6]

In Sec. II, which follows, simulations are presented which have some features of the experiment. The stagnated plasma expands and contracts during the stagnation time t_s, which is comparable to about twice the stagnation radius r_s divided by the Alfvén speed. The kinetic energy is of order of the pressure energy, which is $(Z+1)$ times the ion pressure. In the simulations, the stagnation process is at first not turbulent; turbulence is introduced to the stagnation region by collision of the expanding stagnation shock with the incoming Rayleigh Taylor unstable magnetic piston. In Sec. III, the stagnation radius r_s is calculated, which depends on β, the ratio of pressure energy to magnetic energy. A simple expression for the stagnation radius r_s is obtained which agrees with simulations. The effect of radiative loss on r_s is calculated, using a simple radiation model, and is also in agreement with simulations. Conclusions are presented in Sec. IV.

II. SIMULATIONS

Simulations were done with an adaptation of the M3D (Ref. 14) code. This code has been primarily applied to tokamak magnetic fusion devices. More recently, the code has been applied to highly turbulent simulations, such as disruptions[15] and edge localized modes (ELMs).[16] In these simulations, strong advection was present. Upwind numerical methods[17] were introduced to deal with advection. This made it possible to also simulate Z pinches in which advection is dominant. The code has the advantage of allowing mesh refinement in two directions (r, z),[18] which is helpful in trying to find short wavelength turbulence, expected to occur in Z pinch stagnation. Two dimensional simulations were performed in cylindrical geometry.

The code solved the resistive MHD equations

$$\rho\frac{\partial \mathbf{v}}{\partial t} = -\rho\mathbf{v}\cdot\nabla\mathbf{v} - (\nabla\times\mathbf{B})\times\mathbf{B} - \nabla p + \mu\nabla^2\mathbf{v}, \quad (1)$$

$$\frac{\partial \rho}{\partial t} = -\nabla\cdot(\rho\mathbf{v}), \quad (2)$$

$$\frac{\partial \mathbf{B}}{\partial t} = \nabla\times(\mathbf{v}\times\mathbf{B}) + \eta\nabla^2\mathbf{B}, \quad (3)$$

$$\frac{\partial T}{\partial t} = -\mathbf{v}\cdot\nabla T - (\gamma-1)T\nabla\cdot\mathbf{v} + Q + \chi\nabla^2 T, \quad (4)$$

$$Q = Q_d + Q_b - Q_{rad}, \quad (5)$$

$$Q_d = \rho^{-1}\mu[(\nabla v_x)^2 + (\nabla v_y)^2], \quad (6)$$

$$Q_b = \rho^{-1}\eta(\nabla\times\mathbf{B})^2. \quad (7)$$

The total pressure is

$$p = \frac{Z+1}{M_i}\rho T, \quad (8)$$

where M_i is the ion mass. A single temperature is used, modeling rapid electron ion temperature equilibration. Here, Z is the effective ion charge. From quasi neutrality, the electron number density is Z times the ion number density. The assumption of equal ion and electron temperatures gives Eq.

(8) for the sum of ion and electron pressure. In the simulational example given below, $Z=9$. It is assumed that $\gamma=5/3$.

Radiation was treated using a simplified model, in which Q_{rad} was chosen so that the temperature was not allowed to exceed a critical temperature T_c, modeling strong K shell radiation. If the temperature was below T_c, then $Q_{rad}=0$. The temperature was adiabatic for $T<T_c$, while for $T=T_c$ the temperature was isothermal.

In the two dimensional example the magnetic field is

$$\mathbf{B}=(0,0,B),$$

where a (left handed) cylindrical coordinate system (r,z,ϕ) is employed. The equations are in dimensionless form.[14] Length, magnetic field, and density are in arbitrary units. Velocity is in terms of Alfvén speed v_A, and time is length units divided by the Alfvén speed. Constant axial current boundary condition is used. The idea is to make the simplest model qualitatively like the experiment, in order to understand what is happening.

The numerical method uses finite element discretization on an unstructured mesh.[18] In the present simulations, the mesh is uniform, with triangular or rectangular elements. Advection is treated with a flux limited upwinding method for unstructured meshes.[17]

The dissipation coefficients are μ, the viscosity, η, the resistivity, and χ, the thermal conductivity. In the examples shown here, a finite element mesh was used of 100×280 meshpoints, with the region $r<0.2L$ refined in both the r and z directions to give a local effective resolution of about 1000×800 meshpoints. The radius R is twice the axial width L, $R=2L$. The dissipative terms were solved implicitly. The viscosity was $\mu=10^{-5}$, the resistivity η was 10^{-5}, and the thermal conductivity $\chi=10^{-5}$. Spatially constant dissipation coefficients were taken for simplicity. These values were chosen in order to minimize possible stabilization of short wavelength instabilities. Similar results were obtained with the values of dissipation coefficients given in Sec. I. The results are not sensitive to the values of viscosity.

The initial normalized mass density was of the form

$$\rho=\rho_0[0.5-.45\tanh((r-r_1)/\Delta)],$$

where $r_1=1.85L, \Delta=0.02L$. Simulations with a more hollow density profile do not change the qualitative conclusions reported below. Hence, a relatively simple model was chosen to avoid consideration of detailed dependence on initial conditions. The initial temperature was taken to be a constant, $T=T_0$. The initial magnetic field was

$$B=0.5B_0[1+\tanh((r-r_1)/\Delta)]/r.$$

$B_0=0.5, \rho_0=1$, so the Alfvén speed is 0.5. The spatial unit is $L=1$ cm, so the Alfvén time $\tau_A=L/v_A=2$.

The magnetic field boundary condition maintains an axial constant plasma current I. Simulations with an axial current which rises in time change the time evolution quantitatively but not qualitatively. Hence, a constant in time current was chosen for simplicity.

The magnetic field is given by

$$B=I/r. \tag{9}$$

The magnetic field vanishes at $r=0$, so that total current is measured by I at the outer boundary $r=R$. In the implosion phase, I is approximately spatially constant between $R>r>r_B$, where r_B is the radius of the maximum of the z-average of B, which is approximately the magnetic front.

The initial velocity perturbation is a function of position localized in the range $r_1<r<R$. The initial amplitude is $0.05v_A$. The perturbation is both "random," oscillating from grid point to grid point, and includes a non random sinusoidal perturbation.

When the magnetic field pushes on the plasma, it starts to form a high density layer, as in the snowplow effect. However, the pressure prevents the density from becoming too high. Instead a shock forms ahead of the magnetic field, as seen in Fig. 1. The front of the shock is stable, but the back of the high density region, where it is pushed by the magnetic piston, is Rayleigh Taylor unstable. Fig. 1(a) shows the z-averaged magnetic field B at several times during the implosion and stagnation. Also shown in Fig. 1(b) is the z-averaged density ρ at the same time.

Contour plots of B and ρ are shown in Fig. 2, before the shock reaches the origin. The magnetic piston front in Fig. 2(a) is perturbed by the Rayleigh Taylor instability. The shock front in Fig. 2(b) is unperturbed, while the interface with the magnetic piston is perturbed along with the magnetic field.

The condition for Rayleigh Taylor instability in a slab is

$$g\rho'<0,$$

where the effective gravity $g=vv'$ and the primes denote radial derivatives. This is satisfied at the piston front, where $vv'>0$ and $\rho'<0$, but not at the shock front, where both $vv'>0$ and $\rho'>0$. The shock reaches the axis ahead of the magnetic field and starts the stagnation phase.

The stagnation is caused by the buildup of pressure on axis, which causes a pressure force on axis to oppose the inward magnetic and inertial forces. After the shock reflects from the origin, it propagates outwards. It encloses the high density plasma which reaches the origin. It can be denoted the stagnation shock. It is unmagnetized and expands relatively slowly. During the expansion the shock front is stable, with both $vv'<0$ and $\rho'<0$.

Contour plots of B and ρ are shown in Fig. 3, at time $t=3.4\tau_A$, after the shock reflects from the origin, halfway through the stagnation phase. The magnetic piston front in Fig. 3(a) is perturbed by the Rayleigh Taylor instability. The density in Fig. 3(b) is perturbed at the magnetic piston interface but the origin is relatively unperturbed. At this time, the density has expanded to its maximum stagnation radius.

The implosion and stagnation of the plasma column is shown in Fig. 4, which shows the radii r_B, r_{n1}, r_{n2} as a function of time. The radius r_B is defined as the radius of the maximum value of the z-average of B. This a reasonable

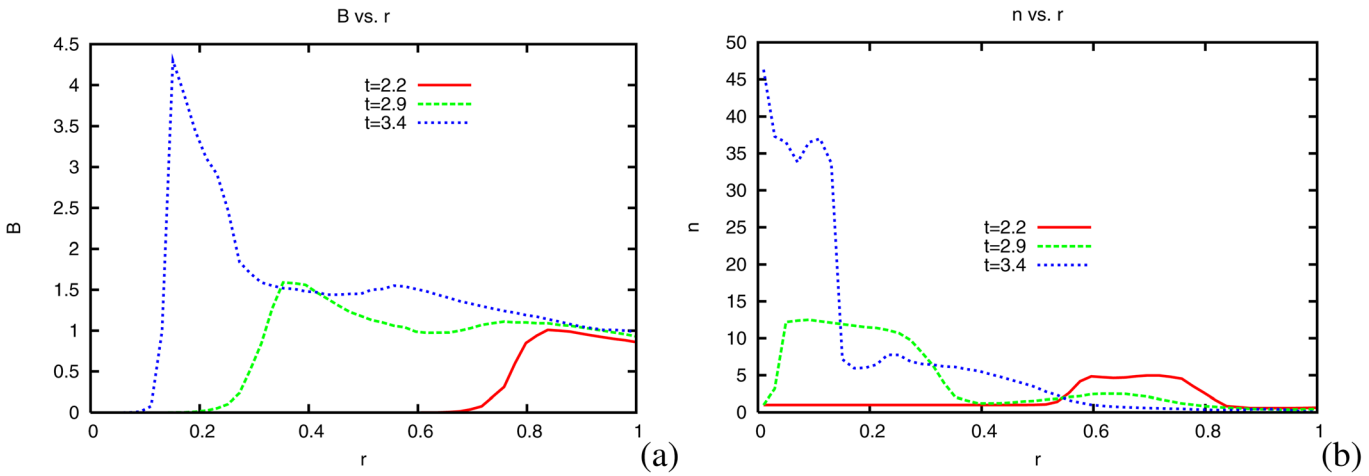

FIG. 1. (a) Magnetic field B, averaged in z, as a function of r, at times $t = 2.2\tau_A, 2.9\tau_A, 3.4\tau_A$. (b) Density ρ, averaged in z, as a function of r, at same times. The high density region at $t = 2.9\tau_A$ has not quite reached the origin. It is bounded on the left by the shock radius r_{n1} and on the right by the radius r_{n2}, adjacent to magnetic piston. At later times, the high density has reached the origin and $r_{n1} = 0$, while r_{n2} is the width of the high density stagnated core.

measure of the magnetic piston radius. The density is described by two radii. The peak value of the z-averaged density has radius $r = r_{n1}$. During implosion, it is the shock radius. The radius of the half maximum z-averaged density is r_{n2}. During implosion, it is somewhat less than the magnetic piston radius r_B. During stagnation, it is the radius of the reflected shock wave, which first reflects from the origin and then from the magnetic piston. Hence, it is always the case that $r_{n1} \le r_{n2} \le r_B$. The radius r_{n1} stays at zero during stagnation because the density is maximum on axis. Experimental observations are made of the radius r_r, the average maximum radius of temperature $T = T_c$, as defined in Eq. (4). This is the radius of the strongly radiating high temperature plasma. In the simulations, the radius r_r expands, reaches radius r_B, and then contracts. The time scale for the plasma to expand is $(r_s/L)\tau_A = 0.3$ in dimensionless units, taking r_s equal to the minimum value of r_B or the maximum value of r_r. If the stagnation time t_s is taken to be $0.7\tau_A$, then $t_s = 2.3r_s/v_A$, which is close the experimental value $t_s = 2.4r_s/v_A = 10$ns given in the Introduction.

The total kinetic energy drops at stagnation. Shown in Fig. 5 are the total ion kinetic energy KE and the total pressure P, as a function of time,

$$KE = \frac{1}{2}\int\int \rho v^2 r dr dz, \tag{10}$$

$$P = \frac{1}{\gamma - 1}\int\int p r dr dz. \tag{11}$$

The radiated energy, the viscously dissipated energy, and the ohmically dissipated energy are all less than 0.05 P, hence

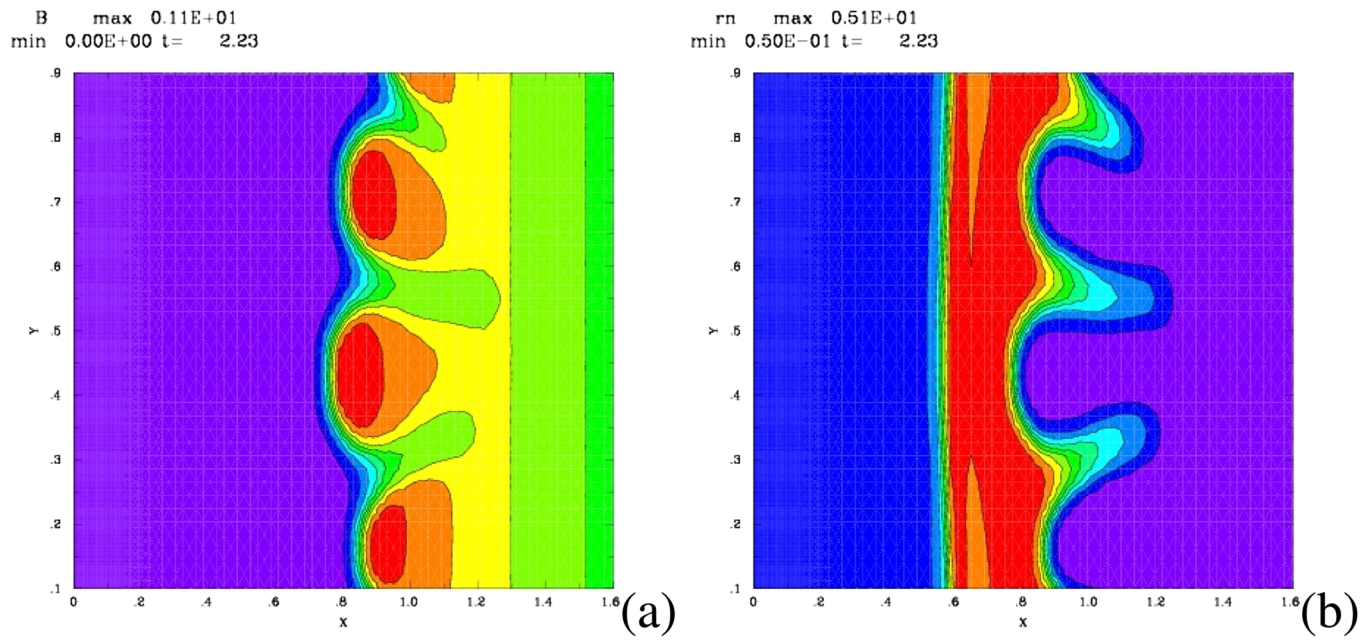

FIG. 2. (a) Magnetic field B at time $t = 2.2\tau_A$. The magnetic front to the left is the magnetic piston. It is rippled by the Rayleigh-Taylor instability. (b) Density ρ at same time. This is near the end of the implosion phase. The shock is on the left side of the high density density region, while the unstable piston interface is to the right.

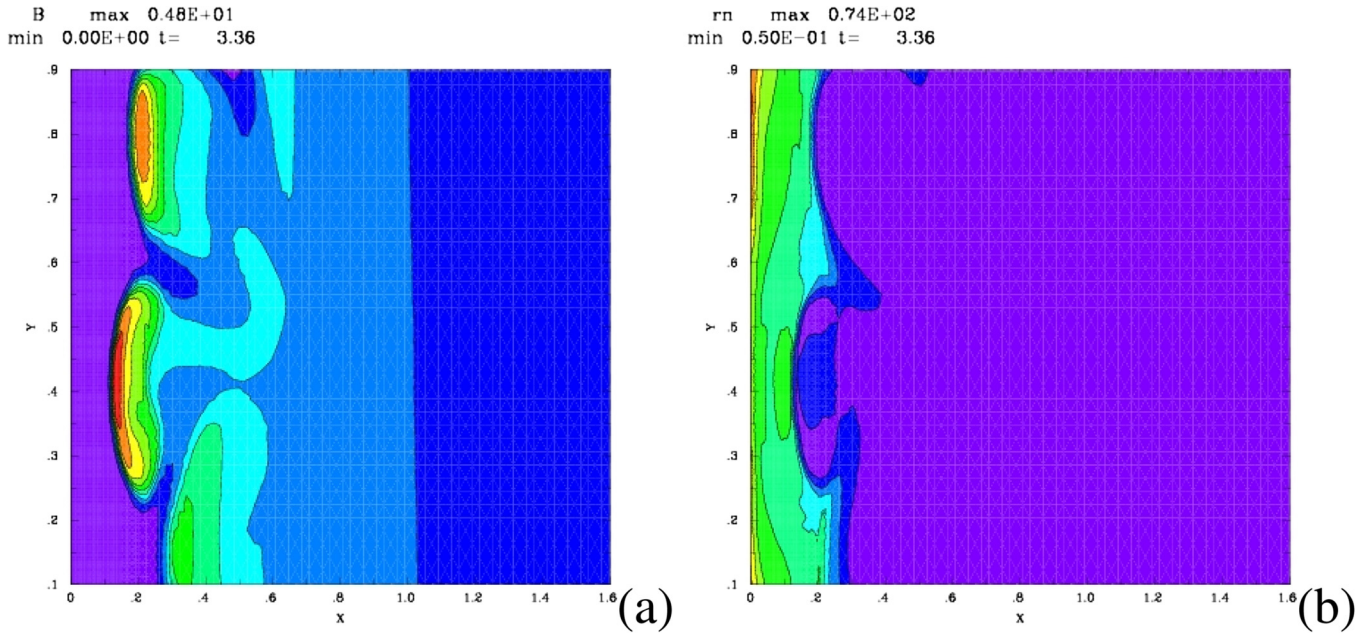

FIG. 3. (a) Magnetic field B at time $t = 3.4\tau_A$, in the stagnation phase. (b) Density ρ at the same time.

negligible compared to the total pressure. Even with the larger dissipation coefficients mentioned in the Introduction, the heating is still relatively unimportant. The drop in kinetic energy corresponds to a rise in plasma pressure, evidently related to pdV compression of the plasma, rather than dissipation.

The ion pressure $P_i = P/(Z+1)$, is also shown in Fig. 5, where $Z=9$ as in the experiment described in the Introduction.[6] At the beginning of stagnation, the kinetic energy is comparable to the pressure and is about $(Z+1)$ times the ion pressure. This is consistent with experimental observations[6] as presented in the Introduction. After reaching the origin, the ion kinetic energy is comparable to the plasma pressure in the stagnated unmagnetized region

$$\frac{1}{2}\rho v_i^2 \approx p. \tag{12}$$

Hence from Eq. (8),

$$\frac{1}{2}M_i v_i^2 = (Z+1)T. \tag{13}$$

The kinetic energy per ion is $Z+1$ times the temperature.

This scaling might be confirmed by carrying out a sequence of simulations with different Z. However, Eqs. (1), (2), and (3) do not contain Z explicitly. The same initial profiles of ρ, B, p, and $\mathbf{v}$ will give the same time dependent evolution. From Eq. (8), T must be scaled as $(Z+1)^{-1}$ to give the same pressure.

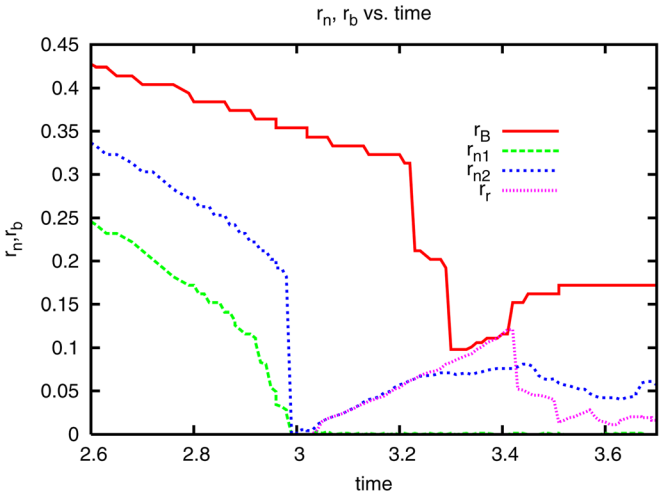

FIG. 4. Pinch radius, as determined from magnetic field r_B, shock radius r_{n1}, density column r_{n2}, and radiative radius r_r as a function of time. At stagnation, the shock radius reaches the origin and becomes zero. The density column radius r_{n2} expands to meet the magnetic radius r_B and is reflected back toward the origin. The radiative radius r_r also expands to r_B and then shrinks.

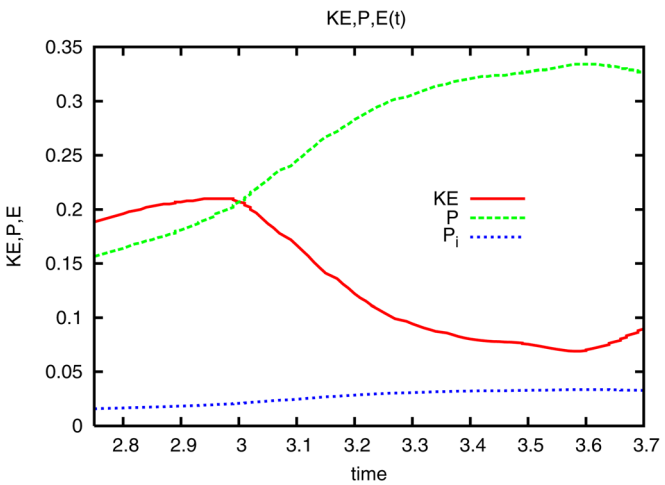

FIG. 5. Shown is the total ion kinetic energy KE and the total pressure P as a function of time. Also shown is the ion pressure $P_i = P/(Z+1)$, where $Z=9$, hence $P_i = 0.1P$. At the beginning of stagnation, the kinetic energy is comparable to the pressure.

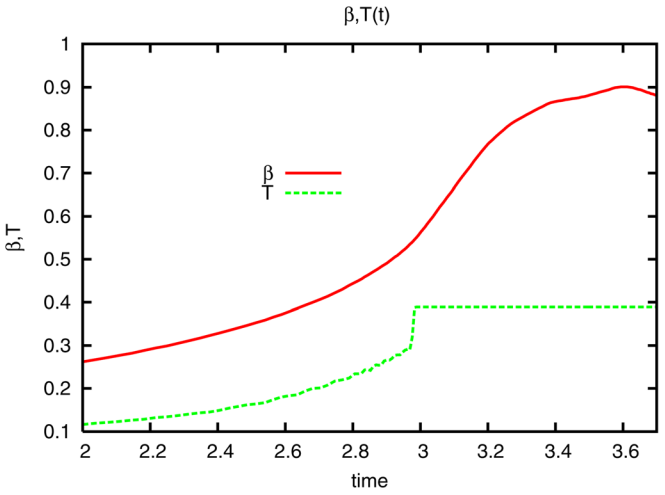

FIG. 6. Time history of β and T in a simulation. While the plasma is imploding, $\beta < 1$. At the beginning of stagnation, $\beta \gg 1$. It then settles down to $\beta \approx 1$, at about $t = 3.4\tau_A$, indicating approximate equilibrium. Also shown is the peak temperature T_{max} in arbitrary units. The peak temperature reaches T_c at $t = 3.0\tau_A$, just before stagnation. The time dependence of β and T is almost the same until stagnation, indicating adiabatic compression.

III. STAGNATION RADIUS

Section II showed that the laminar inflow kinetic energy is comparable to the pressure energy in the beginning of stagnation. In turn the pressure is comparable to the magnetic pressure, measured by quantity β, defined below. In a stagnated state, β can be used to obtain the stagnation radius r_s. The agreement between the analytic solution and numerical simulation is a simple test of the computer code. It is also possible to find how radiative loss decreases the stagnation radius.

The compression and stagnation of the plasma depends on the quantity β, the ratio of plasma pressure to magnetic pressure. If the plasma is in equilibrium, it satisfies force balance, from Eq. (1),

$$2\beta r^2 \nabla p + \nabla(I^2) = 0, \tag{14}$$

where the proportionality constant β has been introduced, and I is given by Eq. (9). Integrating over the plasma volume, assuming $\partial p/\partial z = \partial I/\partial z = 0$ at the $z = 0, L$ boundaries and integrating by parts, yields

$$\beta = 4\frac{\int dzdrrp}{I_r^2 L}, \tag{15}$$

where I_r is measured at the outer boundary $r = R$. The quantity β is plotted as a function of time in Fig. 6. During the implosion phase, the magnetic energy density exceeds the plasma pressure, and $\beta < 1$.

The magnetic field and density are compressed approximately adiabatically. Let r_s be the stagnation radius. Then the density scales as

$$\rho \propto r_s^{-2}$$

and the magnetic field scales as

$$B \propto r_s^{-1}.$$

The temperature scales as

$$T \propto r_s^{-4/3},$$

up to the critical compression for which $T = T_c$, at which radiation limits the temperature. The peak temperature as a function of time is shown in Fig. 6. At the beginning of the stagnation phase, the peak temperature reaches T_c and remains there.

It follows that β scales as $r_s^{-4/3}$ for $T < T_c$, and β is independent of r_s for $T = T_c$. Fig. 6 shows that T and β have the same time variation, until the stagnation phase.

The scaling of r_s with β is confirmed in Fig. 7(a). In this case $T_c \gg T_0$, where T_0 is the initial temperature. Then $\beta_s/\beta_0 = (R/r_s)^{4/3}$, where $\beta_s = 1$ is the stagnation β, and β_0 is the initial β. Hence,

$$r_s = \beta_0^{3/4} R. \tag{16}$$

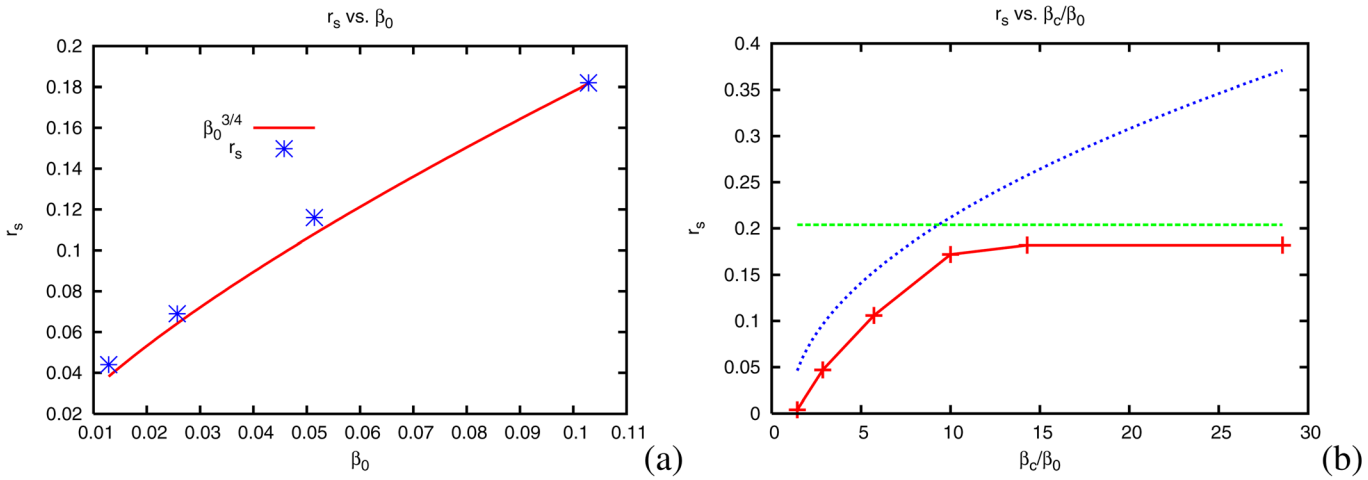

FIG. 7. (a) The stagnation radius, r_s, as a function of initial plasma β_0, with no radiation, $\beta_c \gg \beta_0$. It is well fit by $\beta_0^{3/4}$, indicating that the stagnation radius satisfies $\beta = 1$. (b) The stagnation radius, r_s, as a function of radiation onset β_c/β_0, for fixed β_0. The data are fit by the curves $r_s = \beta_0^{3/4} R$, for $\beta \gg \beta_0$, and by $r_s = (\beta_c - \beta_0)^{1/2}\beta_0^{3/4} R$ for lower β. The point with $\beta_c/\beta_0 = 10$ corresponds approximately to the case in the previous plots.

Because of the scaling of ρ, B, then β depends only on the temperature, $\beta = 2T\rho_0/B_0^2$. In Fig. 7(b), T_0 is constant, while T_c is varied. There is a gradual cutoff of r_s as T_c is reduced. The critical value of T_c occurs when the stagnation temperature equals the radiation onset temperature or when $T_c = T_0\beta_0^{-1}$. In Fig. 7(b), $\beta_0 = 0.12$. so that the critical $\beta_c = 8.33\beta_0$. In this plot, $r_s = r_{n2}$ is the radius at which the plasma first "bounces," when the outgoing reflected shock hits the incoming magnetic piston. The stagnation radius r_s is shown as a function of radiation onset β_c/β_0, for fixed β_0. The data are fit by the curves $r_s = \beta_0^{3/4}R$, for $\beta_c \gg \beta_0$, and by $r_s = (\beta_c - \beta_0)^{1/2}\beta_0^{3/4}R$ for lower β. The rationale for the lower β fit is that the stagnation radius is only a fraction v_s/v_A of the nonradiating radius, where v_s is the effective sound speed in the stagnating column. The effective sound speed is taken proportional to $(T_c - T_0)^{1/2}$.

IV. CONCLUSION

In conclusion, several points have been demonstrated about a gas puff Z pinch resembling the experiment[6] described in the Introduction. The experiment was in a collisional parameter regime. Hence, it could not be the case that the plasma had low collisionality during implosion and then thermalized in an ion-ion collision time at stagnation. Instead, the plasma was well described by MHD during implosion and stagnation. Electron ion thermal equilibration was sufficiently rapid so that ion and electron temperatures were nearly equal. The simulations demonstrated several features in common with the experiment. First, the plasma core in stagnation expands from zero and then contracts, similar to experimental observation.[6] The time scale for this is twice the stagnation radius r_s divided by the sound speed in the stagnated plasma. In turn, the sound speed is comparable to the Alfvén speed, depending on β. Second, the ratio of kinetic energy per ion, to temperature, is determined by balancing ion kinetic energy with pressure in the stagnated core. This gives a ratio of kinetic energy per ion to ion temperature of about $(Z+1)$, where Z is the ion charge. In the neon gas puff of interest, $Z \approx 9$, giving an order of magnitude ratio between the total pressure and the ion pressure. Third, the ion motion in the core, in the beginning of the stagnation phase, is not turbulent. Turbulence is introduced to the stagnation region by collision of the expanding core with the incoming Rayleigh Taylor unstable magnetic piston. Fourth, the stagnation phase reaches a quasi equilibrium with approximate balance of plasma pressure and magnetic pressure, $\beta \leq 1$. Finally, the dependence of the stagnation radius on β and radiation are calculated, using a simple radiation model.

ACKNOWLEDGMENTS

This research was supported by USDOE grant DE-SC0001049. The author thanks Y. Maron and E. Kroupp for helpful discussions.

[1]I. R. Lindemuth and R. E. Siemon, Am. J. Phys. **77**, 407 (2009).
[2]S. A. Slutz, M. C. Herrmann, R. A. Vesey, A. B. Sefkow, D. B. Sinars, D. C. Rovang, K. J. Peterson, and M. E. Cuneo, Phys. Plasmas **17**, 056303 (2010).
[3]D. D. Ryutov, M. S. Derzon, and M. K. Matzen, "The physics of fast Z pinches," Rev. Mod. Phys. **72**, 167 (2000).
[4]M. G. Haines, Plasma Phys. Controlled Fusion **53**, 093001 (2011).
[5]E. Kroupp, D. Osin, A. Starobinets, V. Fisher, V. Bernshtam, Y. Maron, I. Uschmann, E. Förster, A. Fisher, and C. Deeney, Ion-kinetic-energy measurements and energy balance in a Z-pinch plasma at stagnation, Phys. Rev. Lett. **98**, 115001 (2007).
[6]E. Kroupp, D. Osin, A. Starobinets, V. Fisher, V. Bernshtam, L. Weingarten, Y. Maron, L. Uschmann, E. Förster, A. Fisher, M. E. Cuneo, C. Deeney, and J. L. Giuliani, "Ion temperature and hydrodynamic-energy measurements in a Z-pinch plasma at stagnation," Phys. Rev. Lett. **107**, 105001 (2011).
[7]J. D. Huba, *Revised NRL Plasma Formulary* (Naval Research Laboratory, Washington, DC, 2000); E. Stambulchik and Y. Maron, "Plasma formulary interactive," J. Instrum. **6**, P10009 (2011).
[8]D. Osin, Ph.D. dissertation, Weitzmann Institute of Science, 2010.
[9]C. A. Coverdale, C. Deeney, A. L. Velikovich, J. Davis, R. W. Clark, Y. K. Chong, J. Chittenden, S. Chantrenne, C. L. Ruiz, G. W. Cooper, A. J. Nelson, J. Franklin, P. D. LePell, J. P. Apruzese, J. Levine, and J. Banister, "Deuterium gas-puff Z-pinch implosions on the Z accelerator," Phys. Plasmas **14**, 056309 (2007).
[10]J. S. Levine, J. W. Banister, B. H. Failor, N. Qi, H. M. Sze, A. L. Velikovich, R. J. Commisso, J. Davis, and D. Lojewski, "Implosion dynamics and radiative characteristics of a high yield structured gas load," Phys. Plasmas **13**, 082702 (2006).
[11]H. Sze, J. S. Levine, J. Banister, B. H. Failor, N. Qi, P. Steen, A. L. Velikovich, J. Davis, and A. Wilson, "Magnetic Rayleigh-Taylor instability mitigation and efficient radiation production in gas puff Z-pinch implosions," Phys. Plasmas **14**, 056307 (2007).
[12]M. G. Haines, P. D. LePell, C. A. Coverdale, B. Jones, C. Deeney, and J. P. Apruzese Phys. Rev. Lett. **96**, 075003 (2006).
[13]D. Osin, E. Kroupp, A. Starobinets, G. Rosensweig, D. Alumot, Y. Maron, A. Fisher, E. Yu, J. L. Giuliniani, and C. Deeney, "Evolution of MHD instabilities in plasma imploding under magnetic field," IEEE Trans. Plasma Sci. **39**, 2392 (2011).
[14]W. Park, E. V. Belova, G. Y. Fu, X. Tang, H. R. Strauss, and L. E. Sugiyama, "Plasma simulation studies using multilevel physics models," Phys. Plasmas **6**, 1796 (1999).
[15]H. R. Strauss, R. Paccagnella, and J. Breslau, Phys. Plasmas **17**, 082505 (2010).
[16]L. E. Sugiyama and H. R. Strauss, Phys. Plasmas **17**, 062505 (2010).
[17]A. Jameson, "Analysis and design of numerical schemes for gas dynamics 1: Artificial diffusion, upwind biasing, limiters and their effect on accuracy and multigrid convergence," Int. J. Comput. Fluid Dyn. **4**, 171–218 (1995).
[18]H. R. Strauss and W. Longcope, "An adaptive finite element method for magnetohydrodynamics," J. Comput. Phys. **147**, 318–336 (1998).

Appendix B: Notes on Hall MHD Turbulence in a Planar Plasma Opening Switch

H.R. Strauss
HRS Fusion
West Orange NJ 07052

Abstract

We apply two fluid plasma evolution equations a planar plasma opening switch (POS). We find Hall MHD turbulence is excited at the plasma boundary. We show that the propagation of the magnetic field in a planar POS can be explained if the density gradient reverses sign. In that case the magnetic field propagation is insensitive to the magnetic field polarity.

I. Introduction

We study Hall MHD turbulence in a planar plasma opening switch (POS) The relative strength of the Hall term is measured by the Hall parameter H,

$$H = \frac{c}{\omega_{pi} L} = \frac{v_A}{\Omega_i L} \tag{1}$$

where c/ω_{pi} is the ion skin depth, L is a typical length, v_A is the Alfvén velocity, and Ω_i is the ion cyclotron frequency. The MHD limit is $H \ll 1$. In the high density plasma opening switch experiments, $H \approx 1$. Electron MHD is obtained in the limit $H \gg 1$ [8].

When H is of order unity or more, the plasma, which is Rayleigh Taylor unstable, becomes unstable to faster growing Hall Rayleigh Taylor instability [14]. In both cases, the instability criterion is that the density gradient is opposite to the magnetic field gradient. This implies that when there is a snowplow effect, in which density is piled up ahead of a magnetic front, the front of the snowplow is stable [9].

When there is a density gradient transverse to the magnetic front, the Hall effect causes magnetic field penetration [1]. The penetration depends on the polarity of the magnetic field. If the polarity has one sign (positive) the field penetrates, while if it has the opposite (negative) sign, the field is does not penetrate. On the other hand, experimental evidence indicates that penetration (or at least propagation) occurs for either polarity [4]. It was suggested that perhaps Hall Rayleigh Taylor turbulence allowed propagation of the field regardless of polarity [4]. The present results on Hall turbulence show that this is unlikely. The turbulence occurs behind the magnetic front. In a previous study it was shown that the Hall effect tends to be turned off and the motion of the front is dominated by MHD plasma pushing [7]. Here another possibility is suggested, that the density gradient changes sign. In that case penetration will always occur, although depending on polarity, penetration occurs in different regions of the POS. This causes the front to have characteristic wedge shape, which is seen in experiments [4].

II. Two-Fluid Equations

In the experiment reported in [4, 5, 6], there were two ion species, hydrogen and carbon ions. In a previous study, we considered the effects of the relative drift of the ion species and found it made little qualitative difference [7]. In this study, for simplicity, we will study

a single ion species, which in fact could be composed of several species that move with the same MHD velocity, having effective mass μ_Z compared to a proton mass and average charge Ze. The average ion number density is n_Z. From quasineutrality (negligible Debye length), the electron density is

$$n_e = Z n_Z. \tag{2}$$

The electron velocity can be expressed in terms of the current, as

$$\mathbf{v}_e = \mathbf{v} - \frac{H}{n_e}\nabla \times \mathbf{B} \tag{3}$$

where $\mathbf{v}$ is the ion velocity. Here dimensionless variables have been introduced. The magnetic field, density, and length are normalized to typical values. Velocities are expressed in terms of Alfvén speed. The time is expressed in Alfvén transit times $\tau_A = L/v_A$, where L a length. This scaling was used in our previous study [7]. Since the experiments of interest have low plasma pressure relative to magnetic pressure, the plasma pressure will be neglected. The ion momentum equation can be added together with the electron equation to obtain the MHD result,

$$n\frac{\partial \mathbf{v}}{\partial t} + n\mathbf{v}\cdot\nabla\mathbf{v} = (\nabla \times \mathbf{B}) \times \mathbf{B} \tag{4}$$

Here n is given by

$$n = \mu_Z n_Z \tag{5}$$

Neglecting electron pressure and electron inertia, the induction equation gives

$$\frac{\partial \mathbf{B}}{\partial t} = \nabla \times \left[\left(\mathbf{v} - \frac{H}{n_e}\nabla \times \mathbf{B}\right) \times \mathbf{B} - \eta \nabla \times \mathbf{B}\right] \tag{6}$$

where η is the resistivity. The mass density satisfies

$$\frac{\partial n}{\partial t} = -\nabla \cdot (n\mathbf{v})\,. \tag{7}$$

This is a complete set of equations, (4), (6), (7) for the primary variables $\mathbf{v}$, $\mathbf{B}$, n .

III. Hall Rayleigh Taylor Instability

The Hall Rayleigh Taylor instability has been described previously [14].

To analyze stability, assume slab geometry and perturbed velocity

$$\tilde{\mathbf{v}} = (\tilde{v_x}, \tilde{v_y}, 0).$$

It will be assumed that the perturbed quantities have the time and spatial dependence,

$$\tilde{\mathbf{v}} \sim \exp(\gamma t + ikZ).$$

Then (7) becomes

$$\gamma \tilde{n} = -n'\tilde{v}_x - ikn\tilde{v}_y \tag{8}$$

where the prime denotes a derivative with respect to the argument x. Similarly (6) gives

$$(\gamma + \eta k^2)\tilde{B} = -(B' - i\gamma k\frac{H}{Z}))\tilde{v}_x - ikB\tilde{v}_y. \tag{9}$$

The y component of (4) yields

$$\gamma n\tilde{v}_y = -ikB\tilde{B} \tag{10}$$

This can be used to eliminate $\tilde{v}_y$ from (9) to give

$$\left[n\gamma(\gamma + \eta k^2) + k^2B^2\right]\tilde{B} = -n\gamma(B' - i\gamma k\frac{H}{Z}))\tilde{v}_x \tag{11}$$

and from (8) to yield

$$\gamma\tilde{n} = -n'\tilde{v}_x - \frac{Bk^2}{\gamma}\tilde{B} \tag{12}$$

Taking the $\hat{\phi}$ component of the curl of (4) gives

$$\nabla \times (\gamma\tilde{\mathbf{v}} + \mathbf{v}\cdot\tilde{\nabla}\mathbf{v})\cdot\hat{z} = \frac{1}{2n^2}\nabla n \times \nabla B^2 \cdot \hat{z} \tag{13}$$

and substituting (11),(12) yields the dispersion relation

$$(\gamma + \eta k^2 + \frac{B^2k^2}{\gamma n})(\gamma + \frac{BB'n'}{\gamma n^2}) = (B' - ik\gamma\frac{H}{Z})(\frac{B^2B'k^2}{\gamma^2n^2} + \frac{Bn'}{n^2}) \tag{14}$$

There are two limits of interest. The MHD limit is obtained from $H = 0$ and $\gamma^2 \ll k^2B^2/n$. This yields

$$\gamma^2 = \frac{BB'}{n}(\frac{B'}{B} - \frac{n'}{n}) \tag{15}$$

In the MHD limit, stability requires that

$$\frac{n'}{n} > \frac{B'}{B}.$$

It evidently is possible to have an MHD instability if the density gradient has the same sign as the magnetic field gradient. This might happen at the front of a snowplow. However the density gradient cannot become steeper than the magnetic field gradient, or it becomes stable. In the case when the gradients of density and magnetic field have opposite sign, there is MHD instability.

The other limit of interest is the case in which $Hk \gg 1$. This gives the dispersion relation [14]

$$\gamma^2 = -\frac{B'}{n'}Bk^2. \tag{16}$$

If the acceleration is expressed in terms of a gravity

$$g = -B\frac{B'}{n}$$

the dispersion relation becomes

$$\gamma^2 = g\frac{n}{n'}k^2.$$

It is evident from (16) that the instability requires opposite density and magnetic field gradients.

The Hall MHD Raleigh Taylor instability can give a high level of turbulence. A simple quasilinear estimate of the nonlinear saturation is

$$\tilde{v} = \frac{\gamma}{k} = \left(\frac{L_n}{L_B}\right)^{1/2} v_A \tag{17}$$

where the expression (16) was used for the growth rate, $L_B = B/B'$, $L_n = -n/n'$. This shows that the saturated turbulence will have perturbed velocity comparable to the directed energy. There is evidence that this is the case in POS experiments.

IV. Simulation of a Planar Plasma Opening Switch

In this section we show simulations of a model planar plasma opening switch using the equations developed in the previous section. The simulations were done with a substantially modified version of the M3D [12, 13] code. Because of numerical difficulties with low density, the problem of field penetration from a vacuum region into the plasma is not considered here. It is assumed that the field has penetrated into the plasma. The computations are concerned with the propagation of the magnetic field in the plasma. The computations used a 70×70 rectangular mesh. The dimensionless radial width is $L_y = 2L$, and the vertical length is $L_x = 5L$, similar to the experiments [4, 5, 6]. Dissipation is added to the equations: the resistivity was $\eta = 10^{-3} v_A L$, which is about an order of magnitude greater than collisional diffusion [4, 5, 6]. This is compatible with more recent experimental measurements. The initial ion density has a spatial dependence of the form $F(x)G(y)$ where

$$F(x) = [1 - 0.9\tanh((x - x_0)/\Delta)]$$

where $x_0 = .75L_x, \Delta = 0.05L_x$, and

$$G(y) = (1 + 4|(y - y_0)/(L_y - y_0)|)$$

. The y density gradient changes sign at $y = y_0$. In the example $y_0 = 0.3L_y$. The x dependence of the density The effective mass $\mu_Z = 4$, and the effective charge $Z = 1.33$, assuming a mixture of $1/4$ carbon and $3/4$ protons. The magnetic field B has only a z component. The initial magnetic field is proportional to

$$B \propto [1 + \tanh((x - x_0)/\Delta)].$$

The initial velocity is a random function of position localized in the range $x > x_0$. The initial amplitude is $0.01 v_A$.

With the finite element method employed here, there is no need to specify boundary conditions, except for the diffusion term. For this term, a Neumann (zero normal derivative)

boundary condition is used, except for the magnetic field at $y = 0$. There, the magnetic field is held constant in time, $B(x, 0, t) = 1$.

In the following simulations the normalized Hall parameter $H = 4$. Contour plots of the magnetic field are shown in Fig.1. Shown are (a) the initial field B, and (b) the field at time $t = 1.7\tau_A$. The magnetic front advanced into the plasma. The front is laminar, although it is wedge shaped. The front advances fastest where the density is lowest, where the initial density gradient vanishes. At this point the Hall velocity [1] vanishes. Behind the front there are eddy like structures. It would seem that the eddy structures can not play a role in the magnetic front propagation, although they affect the magnetic field behind the front. The corresponding electron density is shown in Fig.2. The times in Fig.2(a) and Fig.2(b) are the same as in Fig.1. The initial density in (a) reverses its vertical gradient and has a larger negative axial gradient. In Fig.2(b) there two effects: the electron density has piled up at the front, and eddy structures have formed. The Rayleigh Taylor instability requires $\nabla B \cdot \nabla n_e < 0$. The instability condition is satisfied at the edge of the plasma. It is of interest to investigate the turbulent velocity associated with the eddies. The plot in Fig.3 is made by checking the $\hat{y}$ component of fluid velocity at every mesh point contained in a box whose vertices are $(x, y) = (L_x/2, L_y/4)$, $(L_x/2, 3L_y/4)$, $(L_x, 3L_y/4)$, $(L_x, L_y/4)$. The mesh point is added to a bin whose velocities are in the range $(n)dv < v_y < (n + 1)dv$, where $dv = (v_{ymax} - v_{ymin})/N$ and $0 < n < N$. The main feature is a broadened non zero velocity. In Fig.3 (a) are plotted the initial axial velocity distribution. The average velocity is nearly zero. The horizontal axis of the figure shows that the velocity is in the range $|v_x| < 0.01v_A$. At the later time Fig.3(b) corresponding to the previous figures, the spectrum has broadened to $v_x > 1.4v_A$, with the peak of the spectrum at $v_x = -0.15v_A$.

In the next series of plots the magnetic field polarity is reversed. The magnetic field is shown in Fig.4(a) at time $t = 1.7\tau_A$. The structure is quite similar to the case of normal polarity, suggesting that the main effect is MHD pushing. The density is shown in Fig.4(b) at the same time, and it is quite similar to Fig.2(b). The spectrum at the same time is shown in Fig.5.

IV. Conclusion

In this paper we have applied two fluid plasma evolution equations to the problem of magnetic field propagation in a planar plasma opening switch. We find that, similar to experiment, there is strong Hall Rayleigh Taylor turbulence at the plasma boundary. The turbulence is behind the front and cannot be responsible for the front propagation. Instead the propagation appears to be largely MHD pushing, which has its maximum velocity where the density is a minimum. When there is density gradient reversal, the front has a wedge shape whose propagation is independent of the polarity of the magnetic field.

Appendix

It is interesting to compare these results to recent experimental POS data [15]. The POS diagnostics were improved to give an order of magnitude better spatial resolution, of about twice the electron skin depth, whose value is $3\times10^{-2}\mathrm{cm}$. This should be adequate to resolve the Hall Rayleigh Taylor modes, whose wavelength should be longer than the electron skin depth. If the modes are damped by gyrovsicosity, the stability condition would be $k\rho_i < 1$,

where ρ_i is the ion gyroradius and k is the wavenumber. In terms of the electron skin depth this condition is

$$k\delta_e(m_i v_A/m_e v_i)^{1/2} = k\rho_i < 1,$$

where v_i is the ion thermal speed, and m_e, m_i are electron and ion masses. The expression in the parentheses is > 1, hence the modes will be damped even for $k\delta_e < 1$.

The magnetic field front was observed to be laminar, with a profile similar to that expected from a snowplow model of magnetic field penetration [8]. The width of the front, $w_B = 0.5\mathrm{cm}$, is consistent with anomalous resistivity, where w_B is the width of the magnetic front. The front moved at about half the Alfvén speed, which was $v_A = 6\times10^7\mathrm{cm\ s^{-1}}$. The ion velocity distribution was measured behind the magnetic front. In the front, the distribution was relatively narrow, while behind the front, the velocity distribution was broad, consistent with the picture of turbulence developing behind the front in Fig.3,Fig.5. If we use the Hall MHD Rayleigh Taylor growth rate (16) then the modes have of order kw_B e - folding times to grow and reach nonlinear saturation. It is possible that $kw_B \approx 10$, which would make the mode wavelength resolvable, although so far the turbulent eddies have not been identified. If we use the simple saturation model (17), then the perturbed velocities of the eddies is comparable to the directed velocity. This is consistent with measurements of the perturbed velocities.

Acknowledgment. This work was supported in part by the U.S. D. O. E. and by the United States - Israel Binational Science Foundation (BSF) Grant No. 2002187.

References

[1] A. Fruchtman, Phys. Fl. **B 3**, 1908 (1991).

[2] A.S. Kingsep, Yu. V. Mohkov, and K. V. Chukbar, Sov. J. Plasma Physics **10**, 495 (1984); A.S. Kingsep, K. V. Chukbar, and V. V. Yankov, in *Reviews of Plasma Physics*, edited by B. Kadomstev, Vol. 16, p. 243 (Consultants Bureau, New York, 1990).

[3] A. V. Gordeev, A.S. Kingsep, and L. I. Rudakov, Phys. Rep. **243**, 215 (1994).

[4] R. Arad, K. Tsigutkin, Y. Maron, A. Fruchtman, J. D. Huba, Observation of faster than diffusion magnetic field penetration into a plasma, Phys. Plasmas **10**, 112, 2003

[5] R. Arad, K. Tsigutkin, Y. Maron, A. Fruchtman, Investigation of the ion dynamics in a multispecies plasma under pulsed magnetic fields, Phys. Plasmas **11**, 112, 2003

[6] R. Doron, R. Arad, K. Tsigutkin, A. Weingarten, A. Starobinets, V. A. Bernshtam, E. Stambulchik, Yu. V. Ralchenko, Y. Maron, A. Fructman, A. Fisher, J. D. Huba, M. Roth Plasma dynamics in pulsed strong magnetic fields, Phys. Plasmas, **11**, 2411 (2004).

[7] H.R. Strauss, R. Doron, R. Arad, B. Rubinstein, Y. Maron, A. Fruchtman, "Magnetic field propagation in a two ion species planar plasma opening switch," Physics of Plasmas **14** 053504 (2007)

[8] A. Fruchtman, Phys. Fluids "The snowplow in plasmas of nonuniform density", **4**, 855 (1992)

[9] A. L. Velikovich, F. L. Cochran, and J. Davis, Suppression of Rayleigh Taylor instability in Z - pinch loads with tailored density profiles, Phys. Rev. Lett **77** 853 (1996).

[10] N. Chakrabarti, A. Fruchtman, R. Arad, Y. Maron, Ion dynamics in a two ion species plasma, Physics Letters A, **297**, 92 - 99 (2002).

[11] A. V. Gordeev, Hydrodynamic model of the penetration of a magnetic field into a plasma with two ion species, Plasma Physics Reports **27**, 659 (2001). Translated from Fizika Plazmy **27**, 700 (2001).

[12] W. Park, E.V. Belova, G.Y. Fu, X. Tang, H.R. Strauss, L.E. Sugiyama, "Plasma Simulation Studies using Multilevel Physics Models" Phys. Plasmas **6** 1796 (1999).

[13] L. E. Sugiyama, and W. Park, "A nonlinear two-fluid model for toroidal plasmas," Phys. Plasma **7** (2000) 4644.

[14] J. D. Huba, J. G. Lyon, and A. B. Hassam, Phys. Rev. Lett. **59**, 2972 (1987).

[15] B. Rubenstein, Interim Report: Investgation of Magnetic Field Penetration into a Relatively Low - Resistivity Plasma, November 2008.

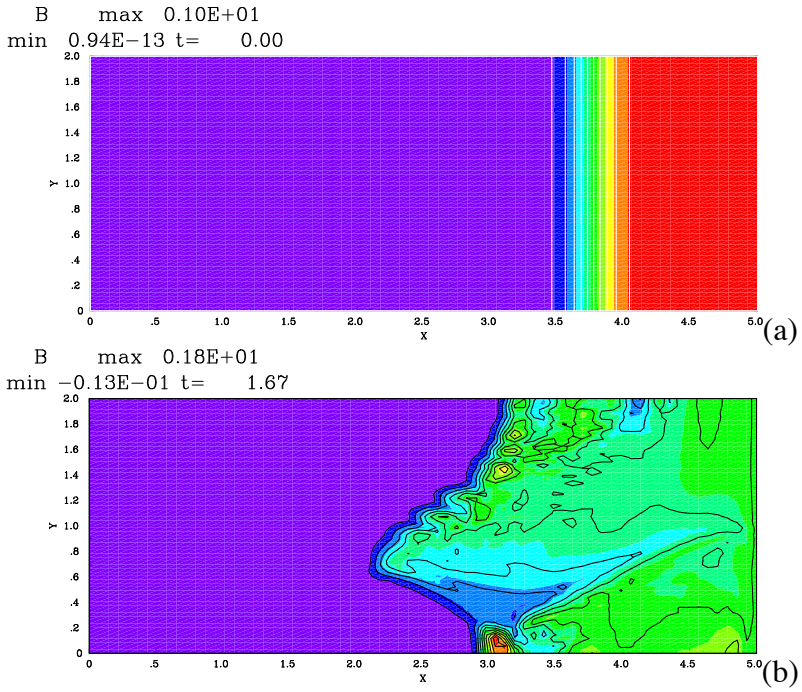

(a)

(b)

Figure 1: magnetic field B at times (a) $t = 0$ and (b) $t = 1.7\tau_A$.

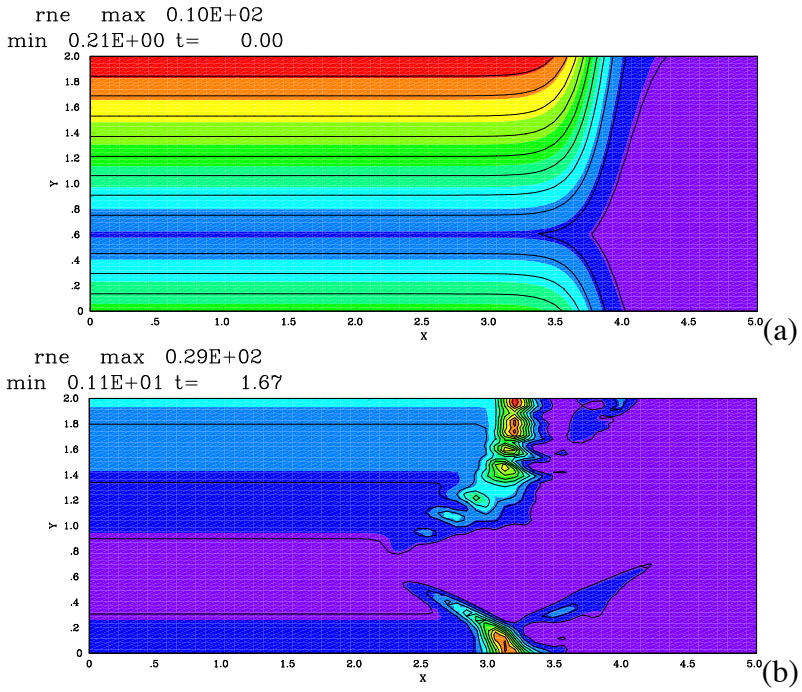

(a)

(b)

Figure 2: electron density n_e at times (a) $t = 0$ and (b) $t = 1.7\tau_A$.

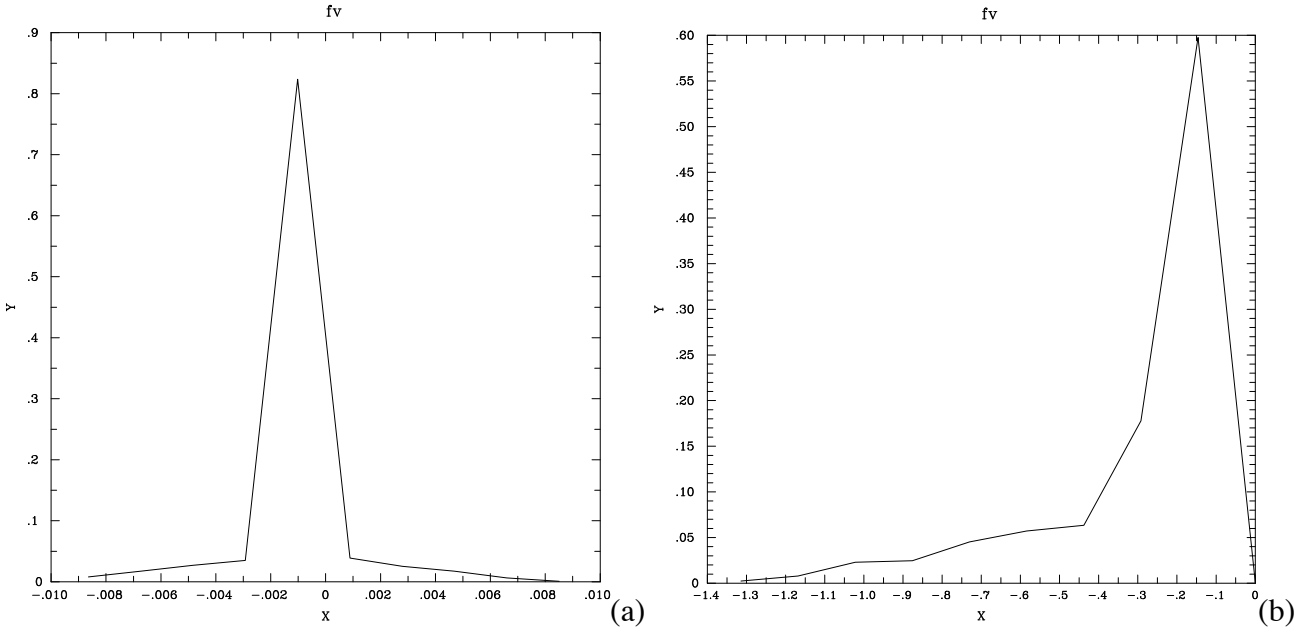

Figure 3: integral energy spectrum at times (a) $t = 0$ and (c) $t = 1.7\tau_A$.

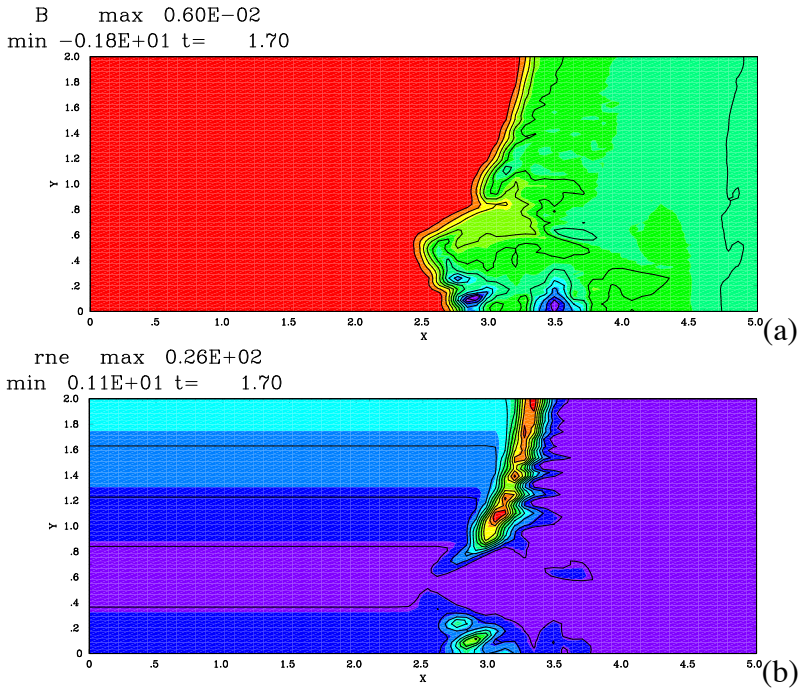

Figure 4: (a) magnetic field B at time $t = 1.7\tau_A$. (b) electron density n_e at time $t = 1.7\tau_A$.

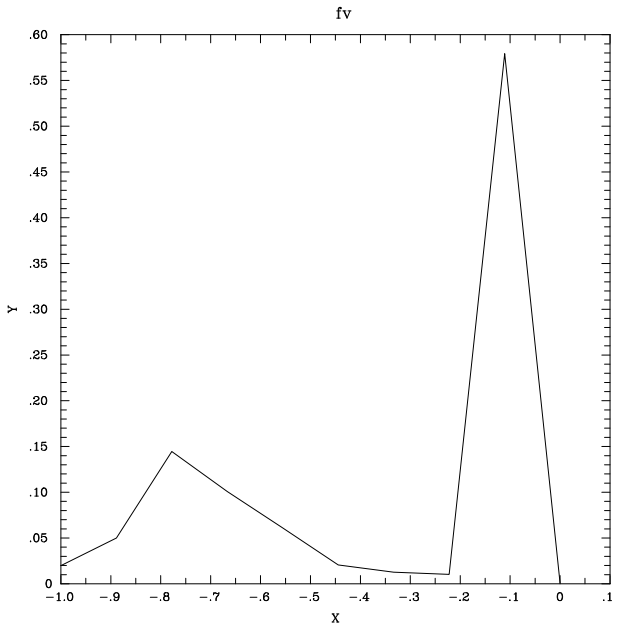

Figure 5: integral energy spectrum at time $t = 1.7\tau_A$.

Appendix C: Finite Temperature Effects in a Three Species Planar Plasma Opening Switch

H.R. Strauss
HRS Fusion
West Orange NJ 07052

Abstract

We apply three fluid plasma evolution equations to a planar plasma opening switch (POS) with two ion species. Finite temperature permits the low mass plasma species to propagate as an unmagnetized shock ahead of the magnetic piston, while the high density species lags behind the magnetic piston.

I. Introduction

We study Hall MHD motion in a planar plasma opening switch (POS). Previous theory has been reasonably successful in explaining features of POS experiments [7, 1]. Several experimental features have been unexplained [15], in particular the following:

1. The current channel width is much wider than predicted [1]. It is measured to be much wider than a resistive diffusion scale or skin depth.

2. Different ion species show different dynamics. The plasma consists of protons and carbon ions. The protons move ahead of the magnetic field front, while the heavy ions are penetrated by the magnetic field and lag behind the magnetic field front.

The two features 1 and 2 can be explained by including finite temperature in the dynamics, which was neglected in previous theory.

An additional feature is that the magnetic field propagation is independent of the sign of the magnetic polarity [4]. It was shown that the Hall term in Ohm's Law tends to be turned off and the motion of the magnetic field front is dominated by MHD plasma pushing [7], which is independent of magnetic polarity.

The relative strength of the Hall term is measured by the Hall parameter H,

$$H = \frac{c}{\omega_{pi} L} = \frac{v_A}{\Omega_i L} \tag{1}$$

where c/ω_{pi} is the ion skin depth, L is a typical length, v_A is the Alfvén velocity, and Ω_i is the ion cyclotron frequency. The MHD limit is $H \ll 1$. In the high density plasma opening switch experiments, $H \approx 1$. Electron MHD is obtained in the limit $H \gg 1$ [8].

When H is of order unity or more, the plasma, which is Rayleigh Taylor unstable, becomes unstable to faster growing Hall Rayleigh Taylor instability [14]. In both cases, the instability criterion is that the density gradient is opposite to the magnetic field gradient. This implies that when there is a snowplow effect, in which density is piled up ahead of a magnetic front, the front of the snowplow is stable [9].

Finite temperature gives a pressure to the snowplow and causes the snowplow to expand. The low mass plasma species propagates as an unmagnetized shock ahead of the magnetic piston, while the high density species lags behind the magnetic piston. The light species can have a velocity much larger than the heavy species, as seen in experiment.

The magnetic field partly penetrates the plasma and partly is carried with it. The variation of the electron velocity between the light and heavy species tends to stretch the magnetic field, giving a large width to the current channel.

Hence, three fluid Hall MHD offers an explanation of the experimental features listed above.

II. Three-Fluid Hall MHD Equations

The derivation of three fluid Hall MHD equations has been given previously [7, 11]. These derivations omitted finite pressure, which is found to have an important effect, and which is included here. In the experiment reported in [4, 5, 6], there were two ion species, hydrogen ions with density n_i and carbon ions with density n_Z and charge Ze. From quasineutrality (negligible Debye length), the electron density is

$$n_e = n_i + Z n_Z. \tag{2}$$

The electron velocity can be expressed in terms of the current, as

$$n_e \mathbf{v}_e = n_i \mathbf{v}_i + Z n_Z \mathbf{v}_Z - H \nabla \times \mathbf{B} \tag{3}$$

Here dimensionless variables have been introduced. The magnetic field, density, and length are normalized to typical values. Velocities are expressed in terms of Alfvén speed. The time is expressed in Alfvén transit times $\tau_A = L/v_A$, where L a length. The scaling is discussed in Appendix A. Neglecting electron inertia, the electron momentum equation is

$$\mathbf{E} + \mathbf{v}_e \times \mathbf{B} = -H \frac{\nabla p_e}{n_e} \tag{4}$$

The dimensionless ion momentum equations are,

$$\frac{\partial \mathbf{v}_i}{\partial t} + \mathbf{v}_i \cdot \nabla \mathbf{v}_i = \frac{1}{H}(E + \mathbf{v}_i \times \mathbf{B}) - \frac{\nabla p_i}{n_i} \tag{5}$$

$$\frac{\partial \mathbf{v}_Z}{\partial t} + \mathbf{v}_Z \cdot \nabla \mathbf{v}_Z = \frac{Z}{\mu_Z H}(E + \mathbf{v}_Z \times \mathbf{B}) - \frac{\nabla p_Z}{n_Z} \tag{6}$$

where μ_Z is the mass ratio m_Z/m_i. The light ion momentum equation (5) can be multiplied by n_i and the heavy ion momentum equation (6) by $\mu_Z n_Z$, and the equations added together with the electron equation to obtain the MHD result, where all the terms are standard except the inertia terms containing $\mathbf{v}_D$,

$$n \frac{\partial \mathbf{v}}{\partial t} + n \mathbf{v} \cdot \nabla \mathbf{v} + \mu_Z \nabla \cdot (\frac{n_i n_Z}{n} \mathbf{v}_D \mathbf{v}_D) = (\nabla \times \mathbf{B}) \times \mathbf{B} - \nabla p + \mu n \nabla^2 \mathbf{v} \tag{7}$$

where $p = p_i + p_Z + p_e$ and μ is a viscosity. The mass density and center of mass velocity have been introduced,

$$n = n_i + \mu_Z n_Z \tag{8}$$

$$n \mathbf{v} = n_i \mathbf{v}_i + \mu_Z n_Z \mathbf{v}_Z \tag{9}$$

along with the difference velocity

$$\mathbf{v}_D = \mathbf{v}_i - \mathbf{v}_Z. \tag{10}$$

Next, the heavy ion equation (6) can be divided by μ_Z and subtracted from the light ion equation (5) to give

$$\frac{\partial \mathbf{v}_D}{\partial t} = \frac{\Omega}{H}\mathbf{v}_D \times \frac{\mathbf{B}}{B} + \mathbf{F} \tag{11}$$

where

$$\Omega = \frac{ZnB}{\mu_Z n_e} \tag{12}$$

$$\begin{aligned}\mathbf{F} = {} & \frac{\mu_Z - Z}{\mu_Z n_e}(\nabla \times \mathbf{B} \times \mathbf{B} - \nabla p_e) - \frac{\nabla p_i}{n_i} + \frac{\nabla p_Z}{\mu_Z n_Z} \\ & -\mathbf{v}\cdot\nabla\mathbf{v}_D - \mathbf{v}_D\cdot\nabla\mathbf{v} - \mu_Z^2\frac{n_Z\mathbf{v}_D}{n}\cdot\nabla\frac{n_Z\mathbf{v}_D}{n} \\ & +\frac{n_i\mathbf{v}_D}{n}\cdot\nabla\frac{n_i\mathbf{v}_D}{n} - \mu\nabla^2\mathbf{v}_D\end{aligned} \tag{13}$$

The electron velocity (3) can be expressed

$$\mathbf{v}_e = \mathbf{v} + (\mu_Z - Z)\frac{n_i n_Z}{n n_e}\mathbf{v}_D - \frac{H}{n_e}\nabla \times \mathbf{B} \tag{14}$$

This can be inserted in the induction equation

$$\frac{\partial \mathbf{B}}{\partial t} = \nabla \times (\mathbf{v}_e \times \mathbf{B} - \eta \nabla \times \mathbf{B}) \tag{15}$$

where η is the resistivity. The mass density satisfies

$$\frac{\partial n}{\partial t} = -\nabla\cdot(n\mathbf{v}) + \chi\nabla^2 n \tag{16}$$

where χ is a diffusion coefficient, and the electron density satisfies

$$\frac{\partial n_e}{\partial t} = -\nabla\cdot\left(n_e\mathbf{v} + (\mu_Z - Z)\frac{n_i n_Z}{n}\mathbf{v}_D\right) + \chi\nabla^2 n_e \tag{17}$$

The ion densities can be obtained from the mass density (8) and electron density (2),

$$n_i = \frac{\mu_Z n_e - Zn}{\mu_Z - Z} \tag{18}$$

$$n_Z = \frac{n - n_e}{\mu_Z - Z} \tag{19}$$

and the ion velocities can be obtained from the mass velocity and difference velocity,

$$\mathbf{v}_i = \mathbf{v} + \frac{\mu_Z n_Z}{n}\mathbf{v}_D \tag{20}$$

$$\mathbf{v}_Z = \mathbf{v} - \frac{n_i}{n}\mathbf{v}_D \tag{21}$$

The pressures are given by

$$p_e = n_e T_e \tag{22}$$
$$p_i = n_i T_i \tag{23}$$
$$p_Z = n_Z T_Z \tag{24}$$

In the following we we assume an isothermal temperature model, although an adiabatic model is also reasonable. In the simulations we will also assume cold ions, $T_i = T_Z = 0$, so that only $T_e = \text{constant}$ is nonzero.

There is now a complete set of equations, (7), (11), (15), (16), (17) (22), (23) (24) for the primary variables $\mathbf{v}$, $\mathbf{v}_D$, $\mathbf{B}$, n, n_e, p_e, p_i, and p_Z. The ion densities n_i, n_Z are derived from (18), (19) and the ion velocities from (20), (21).

The first term on the right hand side of (11) causes the velocity to rotate with angular frequency Ω/H. The other terms correspond to inertial and Lorentz acceleration. The rotation effect appears to be important in making a transition to MHD behavior in a dense planar plasma opening switch. After an initial transient involving rotation, $\mathbf{v}_D$ becomes a drift perpendicular to the magnetic field. In steady state, from (11),

$$\mathbf{v}_D \approx \frac{H}{\Omega B}\mathbf{F} \times \mathbf{B}. \tag{25}$$

Where the plasma is unmagnetized, $B = 0$, then

$$\frac{\partial \mathbf{v}_D}{\partial t} \approx \mathbf{F}.$$

This allows separation of the ion species in unmagnetized regions, an effect which was neglected previously.

III. Simulation of a Planar Plasma Opening Switch

In this section we show simulations of a model planar plasma opening switch using the equations developed in the previous section. The simulations were done with a substantially modified version of the M3D [12, 13] code. Because of numerical difficulties with low density, the problem of field penetration from a vacuum region into the plasma is not considered here. It is assumed that the field has penetrated into the plasma. The computations are concerned with the propagation of the magnetic field in the plasma. The computations used a 50×125 rectangular mesh. The dimensionless height is $L_y = 2L$, and the horizontal length is $L_x = 5L$, similar to experiment [4, 5, 6]. Dissipation is added to the equations: the dimensionless dissipation coefficients were $\eta = \mu = \chi = 10^{-3} v_A L$, which is about an order of magnitude greater than collisional diffusion [4, 5, 6]. This is compatible with more recent experimental measurements. The initial ion densities have a spatial dependence of the form

$$n(x, y) = 1 - c_0 f(x) g(y) \tag{26}$$

where

$$f(x) = 1 - \tanh[(x - x_n)/\delta] \tag{27}$$

and where c_0, x_n, δ are constants given by $c_0 = 0.9, x_n = 4L, \delta = .05L$. and

$$g(y) = 1 + qy/L_y \tag{28}$$

The effective mass $\mu_Z = 12$, and the effective charge $Z = 2.7$. The initial heavy ion density n_Z is $1/Z$ of the initial light ion density n_i, so the two species contribute equally to the electron density n_e. The magnetic field B has only a z component. The initial magnetic field is proportional to

$$B \propto 1 + \tanh((x - x_B)/\delta). \tag{29}$$

where $x_B = 4.5L$.

The initial velocity is a random function of position localized in the range $x > x_0$. The initial amplitude is $0.01v_A$.

With the finite element method employed here, there is no need to specify boundary conditions, except for the diffusion term. For this term, a Neumann (zero normal derivative) boundary condition is used, except for the magnetic field at $y = 0$. There, the magnetic field is held constant in time, $B(x, 0, t) = 1$.

In the following simulation the normalized Hall parameter $H = 1$. The normalized electron temperature is $T_e = 0.1$. Contour plots of the magnetic field and density are shown in Fig.1. Shown are (a) the initial field B, and (b) the initial light ion density n_i. The initial heavy ion density n_Z has the same contours as n_i, but rescaled by a factor $1/Z$. The initial axial profiles in the midplane, $B(x, L_y/2), n_i(x, L_y/2), n_Z(x, L_y/2)$, are shown in Fig.2.

At time $t = 7.1\tau_A$, the contours of B, n_i, n_Z are shown in Fig.3. The axial profiles in the midplane, at the same time, are shown in Fig.4. The light ion density has advanced furthest. It has a broad axial profile. The magnetic field lags behind. Further behind the magnetic field, is the heavy ion density n_Z.

The separation of the two ion species requires nonzero H. The case of $H = 0, T_e = 0.1$ is shown in Fig.5, at time $t = 7.85\tau_A$. Here the heavy ions move together with the light ions.

The case of $H = 0, T_e = 0$ is shown in Fig.6, at time $t = 6.33\tau_A$. The light ions and heavy ions are pushed together in a thin layer ahead of the magnetic field.

The ions are much more peaked when the temperature $T_e = 0$. The case of $H = 1, T_e = 0$ is shown in Fig.7, at time $t = 5.14\tau_A$. The light ions are pushed in a thin layer ahead of the magnetic field. The heavy ions lag behind the magnetic front.

The three fluid equations support three velocities of moving shock like structures: v_B, the magnetic piston velocity v_e (3); v_i, the light ion species velocity (20); and v_Z, the heavy ion species velocity (21). Nearly always $v_i > v_Z$. The magnetic front velocity is typically less than or equal to the light ion velocity, $v_i \geq v_B$. In the following, the initial heavy ion density n_Z is $1/\mu_Z$ of the initial light ion density n_i. The magnetic front velocity is mostly a fraction the Alfvén velocity in addition to a small contribution from the Hall velocity. It was shown in previous work [7] that the Hall velocity tends to vanish, because

the density gradient tends to align with the magnetic field. The field penetration comes from the difference velocity v_D, which causes the heavy ions to be penetrated by the magnetic field and lag behind the magnetic front.

A qualitative understanding of these results can be developed as follows. Assume all quantities are planar, i.e. functions of x only. Hence q will not be considered. Assume that the magnetic piston and plasma species are moving at a speed $v_0 = -B_0/n_0^{1/2}$, the average Alfvén speed of the piston. Now let $v = v_0 + v_1$ ahead of the piston. In the moving frame of the piston, from (7), $B = 0$ and

$$\frac{\partial v_1}{\partial t} + v_1 \frac{\partial v_0}{\partial x} = -\frac{T_e}{n}\frac{\partial n}{\partial x}$$

Substituting for v_0, and assuming that v_1 is time independent and $n \approx n_0$, yields

$$v_1 = -2\frac{c_2^2}{v_0}$$

where $c_s = T_e^{1/2}$, the sound speed. Hence, if the pressure is neglected, v_1 and the MHD velocity is the same as the piston velocity. If $H = 0$, there is no difference velocity, $v_D = 0$. The light and heavy ions move together. If $H \neq 0$, the difference velocity equation (11) is almost the same as (7) when $\mu_Z >> Z$. Hence behind the piston, $v_D \approx v$. If $v_i >> \mu_z v_z$ ahead of the piston, then $v \approx v_i$. Since $v_D = v_i - v_Z \approx v_i$, then $v_Z \approx 0$. Hence, ahead of the piston, $n_Z, v_Z \approx 0$.

Behind the piston, from (25), $v_{Dx} = 0$. Hence light and heavy ions move together at the piston speed. The magnetic field is also advected at the speed v_0. The Hall term in (15) vanishes if there is no vertical gradient, $\partial n_e/\partial y = 0$. Similarly the v_D term does not contribute when it is given by (25).

The spreading of the current sheet might be understood as follows. The magnetic field partially penetrates the light and heavy ions. When the light and heavy ions move at different speeds, when $H > 0$, the magnetic field also moves at somewhat different speeds at the top and bottom of the magnetic field front. The magnetic field gradient is stretched out and broadened. Its width becomes comparable to the height of the plasma, as is observed experimentally [4].

To summarize, ahead of the piston, if $T > 0$, the light ions move faster than the piston. If $H = 0$, both ion species move together, as in Fig.5, while if $H > 0$, the heavy ions move with the piston, as in Fig.4. If $T = 0$, then if $H = 0$, both species move at the piston speed, as in Fig.6. Instead of ions moving ahead of the piston, the ion density piles up as in a snowplow. If $T = 0$ and $H > 0$, there is some magnetic penetration of the heavy ions, as in Fig.7, which may depend on a transient effect not described above.

IV. Conclusion

In this paper we have applied two fluid plasma evolution equations to the problem of magnetic field propagation in a planar plasma opening switch. The magnetic field propagates at the Alfvén speed, with only a very small Hall contribution. This is because the Hall term tends to be suppressed, as shown previously [7]. In the presence of finite pressure, the

ions are pushed ahead of the magnetic piston. This can also occur in Z pinch implosions. In the POS, the Hall parameter produces a difference velocity between light and heavy ions. This causes the heavy ions to lag behind the magnetic piston, and for the heavy ions to be penetrated by the magnetic field. The light ion velocity, in the examples given here, is generally about twice the heavy ion velocity, an effect seen in POS experiments.

Acknowledgment. This work was supported in part by the U.S. D. O. E. and by the United States - Israel Binational Science Foundation (BSF) Grant No. 2002187.

References

[1] A. Fruchtman, Phys. Fl. **B 3**, 1908 (1991).

[2] A.S. Kingsep, Yu. V. Mohkov, and K. V. Chukbar, Sov. J. Plasma Physics **10**, 495 (1984); A.S. Kingsep, K. V. Chukbar, and V. V. Yankov, in *Reviews of Plasma Physics*, edited by B. Kadomstev, Vol. 16, p. 243 (Consultants Bureau, New York, 1990).

[3] A. V. Gordeev, A.S. Kingsep, and L. I. Rudakov, Phys. Rep. **243**, 215 (1994).

[4] R. Arad, K. Tsigutkin, Y. Maron, A. Fruchtman, J. D. Huba, Observation of faster than diffusion magnetic field penetration into a plasma, Phys. Plasmas **10**, 112, 2003

[5] R. Arad, K. Tsigutkin, Y. Maron, A. Fruchtman, Investigation of the ion dynamics in a multispecies plasma under pulsed magnetic fields, Phys. Plasmas **11**, 112, 2003

[6] R. Doron, R. Arad, K. Tsigutkin, A. Weingarten, A. Starobinets, V. A. Bernshtam, E. Stambulchik, Yu. V. Ralchenko, Y. Maron, A. Fructman, A. Fisher, J. D. Huba, M. Roth Plasma dynamics in pulsed strong magnetic fields, Phys. Plasmas, **11**, 2411 (2004).

[7] H.R. Strauss, R. Doron, R. Arad, B. Rubinstein, Y. Maron, A. Fruchtman, "Magnetic field propagation in a two ion species planar plasma opening switch," Physics of Plasmas **14** 053504 (2007)

[8] A. Fruchtman, Phys. Fluids "The snowplow in plasmas of nonuniform density", **4**, 855 (1992)

[9] A. L. Velikovich, F. L. Cochran, and J. Davis, Suppression of Rayleigh Taylor instability in Z - pinch loads with tailored density profiles, Phys. Rev. Lett **77** 853 (1996).

[10] N. Chakrabarti, A. Fruchtman, R. Arad, Y. Maron, Ion dynamics in a two ion species plasma, Physics Letters A, **297**, 92 - 99 (2002).

[11] A. V. Gordeev, Hydrodynamic model of the penetration of a magnetic field into a plasma with two ion species, Plasma Physics Reports **27**, 659 (2001). Translated from Fizika Plazmy **27**, 700 (2001).

[12] W. Park, E.V. Belova, G.Y. Fu, X. Tang, H.R. Strauss, L.E. Sugiyama, "Plasma Simulation Studies using Multilevel Physics Models" Phys. Plasmas **6** 1796 (1999).

[13] L. E. Sugiyama, and W. Park, "A nonlinear two-fluid model for toroidal plasmas," Phys. Plasma **7** (2000) 4644.

[14] J. D. Huba, J. G. Lyon, and A. B. Hassam, Phys. Rev. Lett. **59**, 2972 (1987).

[15] B. Rubenstein, Interim Report: Investgation of Magnetic Field Penetration into a Relatively Low - Resistivity Plasma, November 2008.

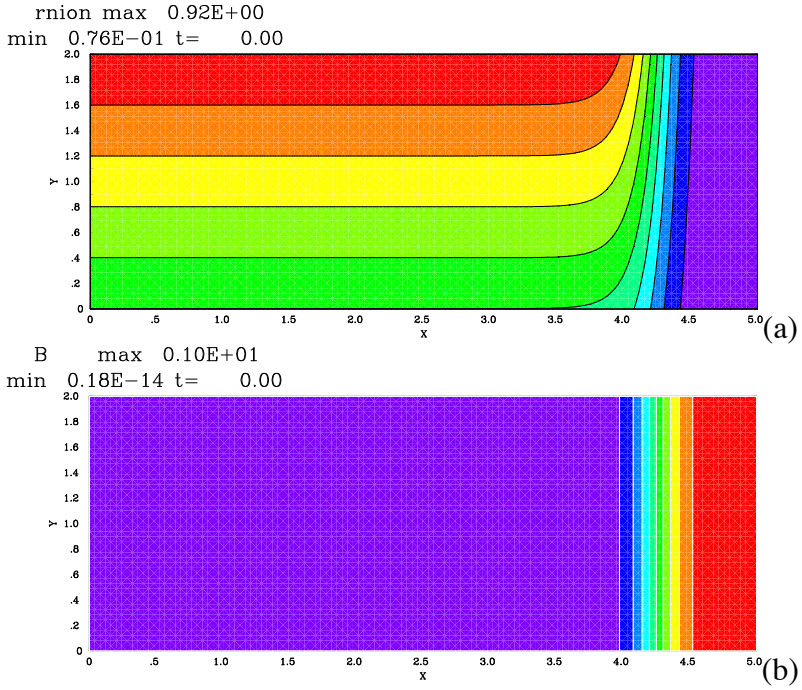

Figure 1: (a) light ion density n_i, (b) magnetic field B, at time $t = 0.0\tau_A$.

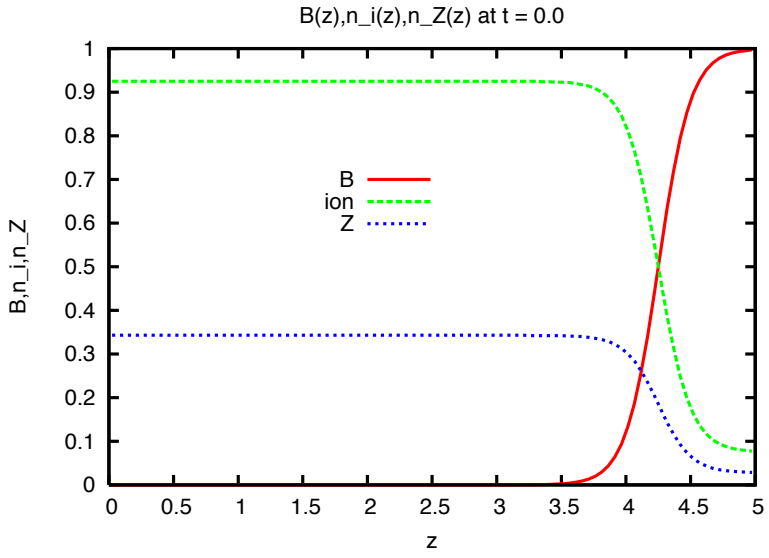

Figure 2: Profiles of light ion density n_i, magnetic field B, and heavy ion density n_Z at time $t = 0.0\tau_A$.
at time $t = 7.60\tau_A$.

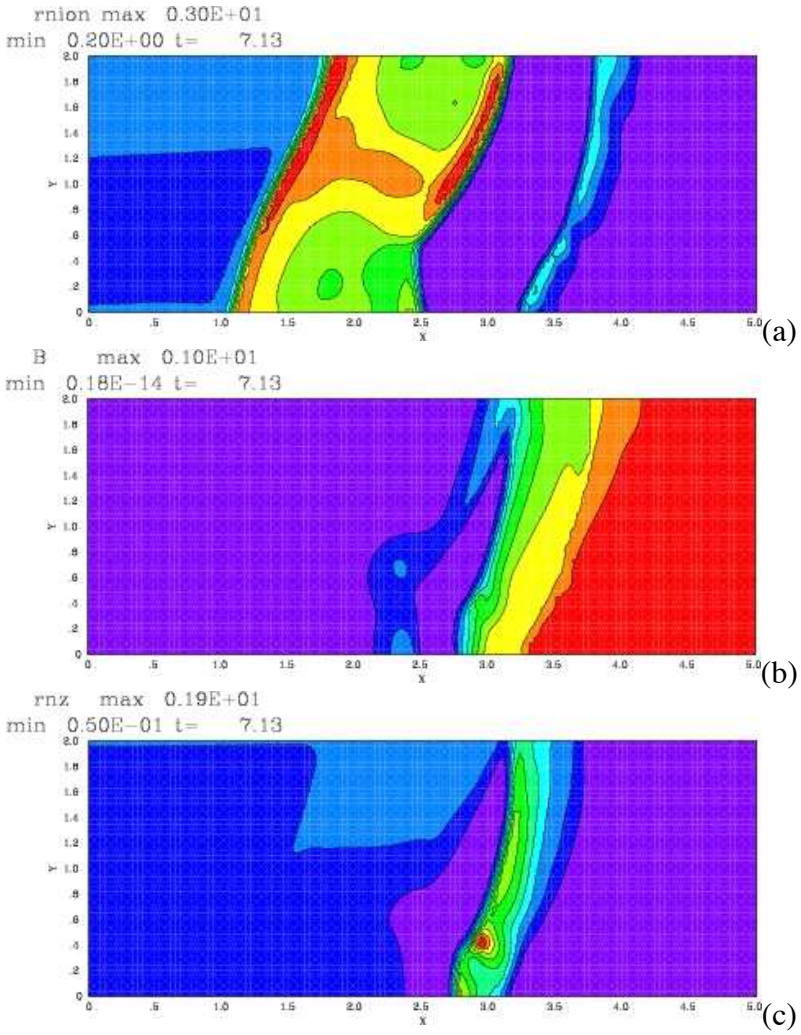

Figure 3: (a) light ion density n_i, (b) magnetic field B, and (c) heavy ion density n_Z at time $t = 7.13\tau_A$. The dimensionless parameters are $H = 1, T_e = 0.1$.

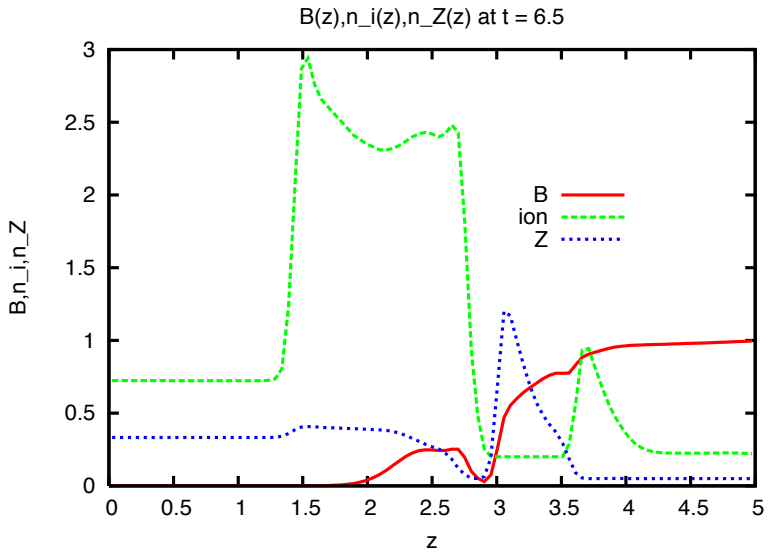

Figure 4: Profiles of light ion density n_i, magnetic field B, and heavy ion density n_Z at time $t = 7.13\tau_A$. The dimensionless parameters are $H = 1, T_e = 0.1$.

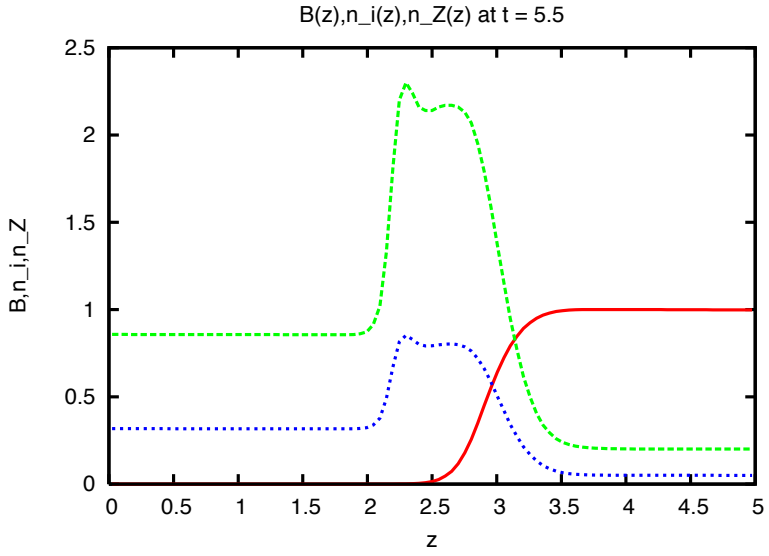

Figure 5: Profiles of (a) light ion density n_i, (b) magnetic field B, and (c) heavy ion density n_Z at time $t = 7.85\tau_A$. The dimensionless parameters are $H = 0, T_e = 0.1$.

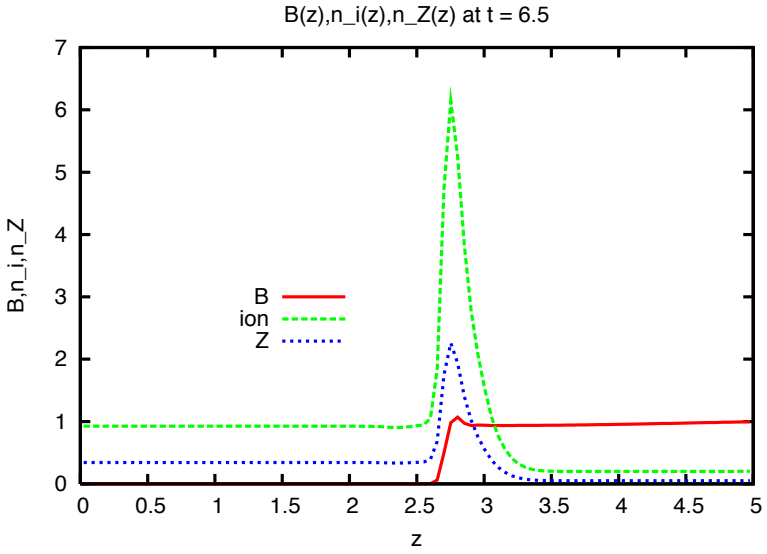

Figure 6: Profiles of light ion density n_i, magnetic field B, and heavy ion density n_Z at time $t = 6.33\tau_A$. The dimensionless parameters are $H = 0, T_e = 0.0$.

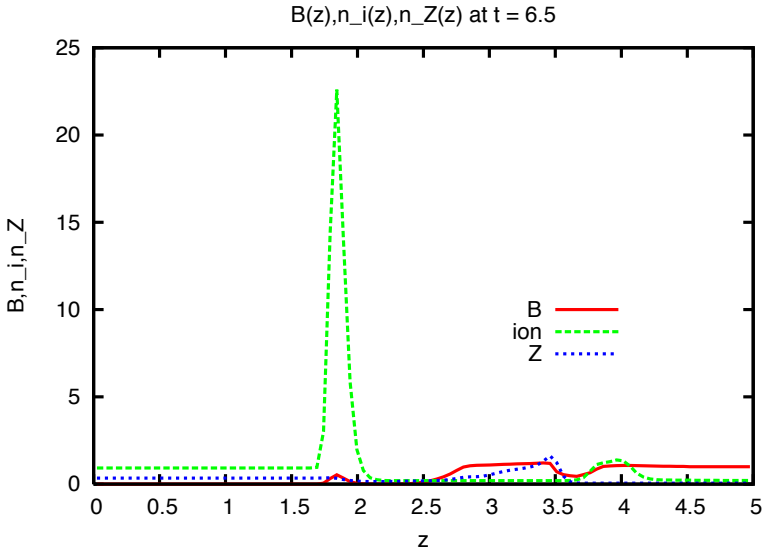

Figure 7: Profiles of light ion density n_i, magnetic field B, and heavy ion density n_Z at time $t = 7.14\tau_A$. The dimensionless parameters are $H = 1, T_e = 0.0$.

Three dimensional simulations of a gas puff Z pinch with an axial magnetic field

H. Strauss

HRS Fusion

ICOPS 10 July 2012

Contents

- Introduction
- Linear stability analysis
  - Rayleigh Tayor stabilization by axial magnetic field
  - Kink / tearing modes destabilized
- Stagnation
  - Axial field inhibits compression
- Nonlinear 3D simulations with M3D code
  - Kink tearing turbulence
- conclusion

Introduction

- Experiment at Weizmann Institute
  - Experiment is about to start operation
  - 500KA Z pinch, with 1 T applied axial magnetic field
  - Plan to measure 3D magnetic fields
  - Related to liner experiments: axial field but no liner!
  - Initial state: plasma is ionized in a spatially constant axial field, then imploded by axial current
- Theory and simulations
  - Will compare predictions with experiment
  - H. Strauss, Stagnation of a gas puff Z pinch, Phys. Plas.19 (2012): 2D simulations of WIS Z pinch without axial field

Model MHD equations

(r, θ, z) coordinates

Assuming azimuthal field $B_\theta \gg B_z$ axial field

$$\vec{B} \approx \nabla \psi \times \hat{\theta} + B_\theta \hat{\theta}$$

$$\vec{v} \approx v\vec{r} + \nabla \phi \times \hat{\theta}$$

$$\rho \frac{d}{dt} \nabla^2 \phi = \vec{B} \bullet \nabla \nabla^2 \psi + \nabla \rho \times (\vec{v} \bullet \nabla \vec{v}) \bullet \hat{\theta}$$

$$\frac{\partial}{\partial t} \psi = \vec{B} \bullet \nabla \phi \qquad J_\theta = -\nabla^2 \psi$$

Strauss, P.F. 20, 1354 (1977)

Rayleigh Taylor stabilization

Assume perturbations vary as $\exp(ik_z z + in\theta)$

and that mode varies more rapidly in z than r, θ

Dispersion relation:

$$(\vec{B}\bullet\vec{k})^2 < \rho' v v' \frac{k_z{}^2}{k_z{}^2 + (n/r)^2}$$

For azimuthal symmetry $n = 0$,

$k_z = 2\pi \mathrm{m/L}$, stable if

$$\frac{B_z}{B_\theta} > \left(\frac{\rho' v v' L^2}{B_\theta^2} \right)^{1/2} \frac{1}{2\pi m} \sim 0.1$$

Axial field does not have to be large to stabilize Rayleigh Taylor

Kink / Tearing mode destabilization

mode varies as $\psi = \psi_1(r)\exp(ik_z z + in\theta)$

$$k_{||}' x(\psi_1'' - k_z^2\psi_1) = k_z \frac{J_\theta'}{B}\psi_1$$

$$\psi_1 = k_{||}' x\phi_1 \;\Rightarrow\; \psi_1(0) = 0$$

where $k_{||} = \vec{B}\bullet\vec{k} / B,\;\; k_{||}(r_s) = 0,\;\; x = r - r_s$

Fourier transform, multiply by $\exp(ik_z x\theta)$ and integrate over x

(ballooning transform) to get a 1st order equation (Strauss, P.Fl. 24, 1981, 2004.)

$$\frac{d}{d\theta}(1+\theta^2)\psi_1 + i\sigma\psi_1 = 0$$

where $\sigma = \dfrac{J_\theta'}{k_{||}' B}$

Kink / tearing 2

solution is

$$\psi_1(x) = \int_{-\pi/2}^{\pi/2} dy \exp(-i\sigma y + ik_z x \tan y)$$

where $y = \tan^{-1}\theta$. The condition $\psi_1(0) = 0$ gives

$$\sigma = 2j, \; j = \text{integer}$$

$$\sigma \approx \frac{L}{\pi n q'} \frac{q''}{[1 + (\pi r q / L)^2]^{1/2}}$$

where $q = \dfrac{B_\theta L}{B_z \pi r}$ analogous to tokamaks

Stagnation radius

Let $r_s =$ stagnation radius, $r_0 =$ initial radius

$\rho \sim r_s^{-2}$, $\mathrm{B}_\theta \sim r_s^{-1}$, $B_z \sim r_s^{-2}$, $T \sim r_s^{-4/3}$

equilibrium condition $p + \frac{1}{2} B_z^2 = \frac{1}{2} B_\theta^2$

neglecting pressure, stagnation occurs for

$B_z = B_\theta$ or $\frac{r_s}{r_0} = \frac{B_{z0}}{B_{\theta 0}} \sim 0.1$

Simulations with M3D code

- M3D used mostly for tokamaks, but allows advection dominated calculations
- Unstructured mesh in (r,z)
- Parallelized with OpenMP and MPI
- Solves full (not approximate) resistive MHD equations

Low axial field example

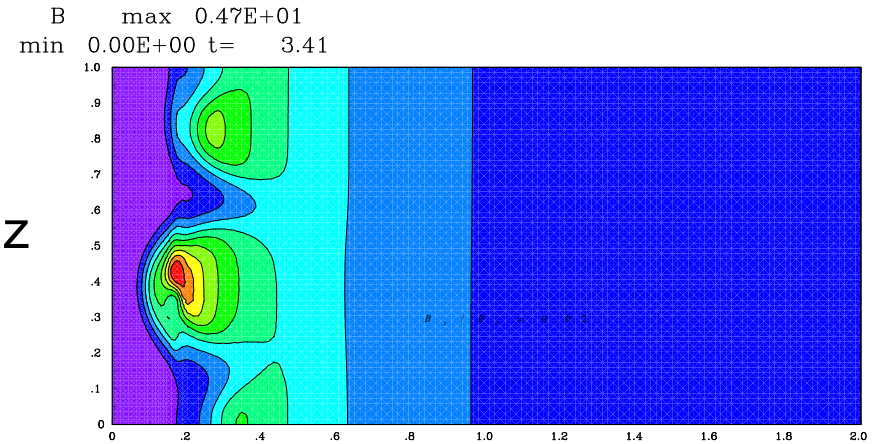

B_θ

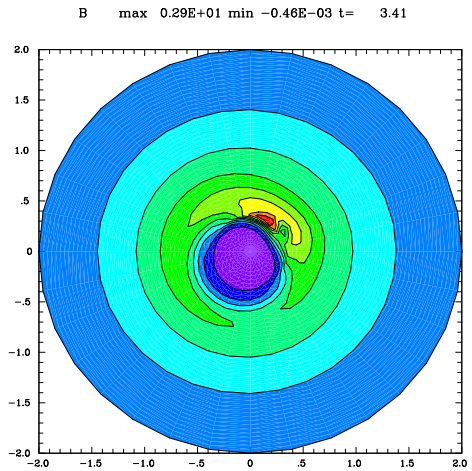

r, θ

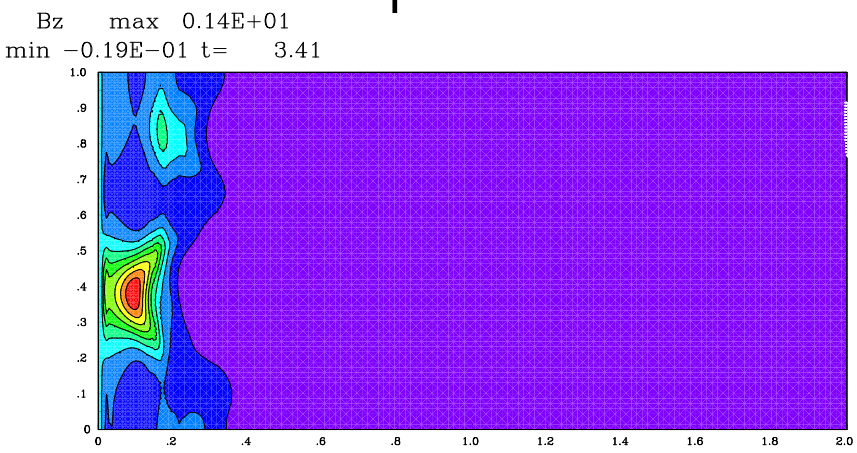

B_z

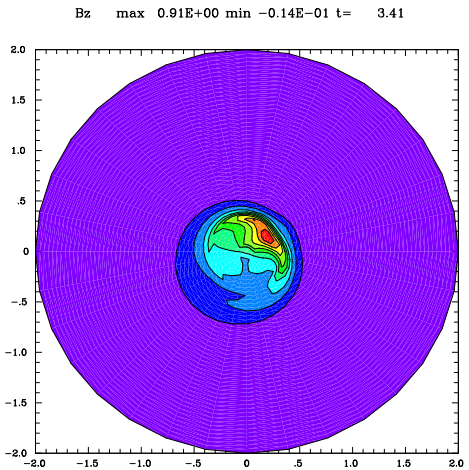

$B_z / B_\theta = 0.02$, RT instability

Higher axial field

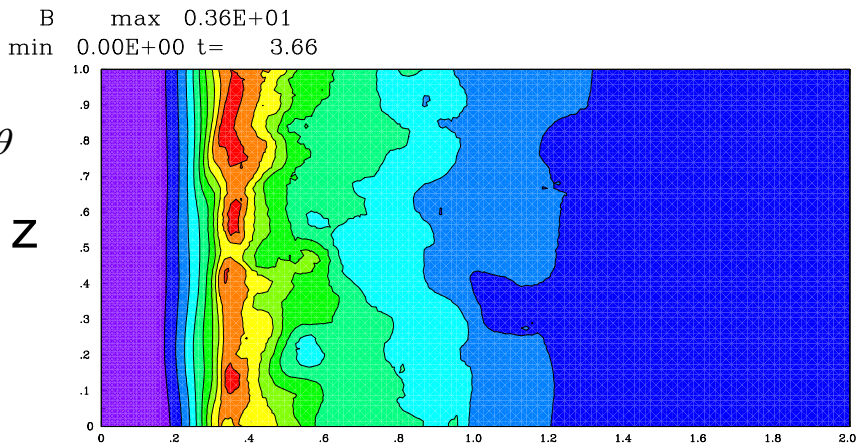

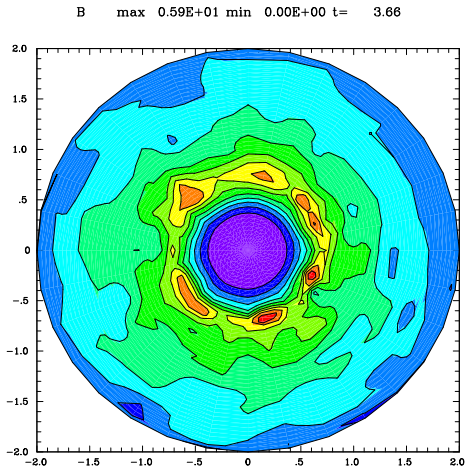

r, θ

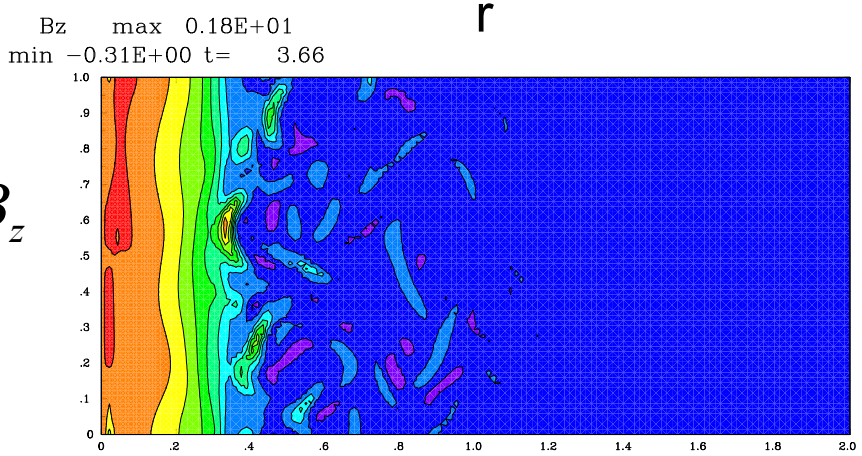

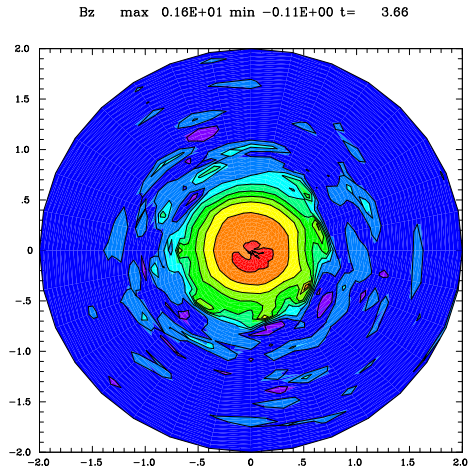

$B_z / B_\theta = 0.10,$ kink instability

Kink / tearing stability

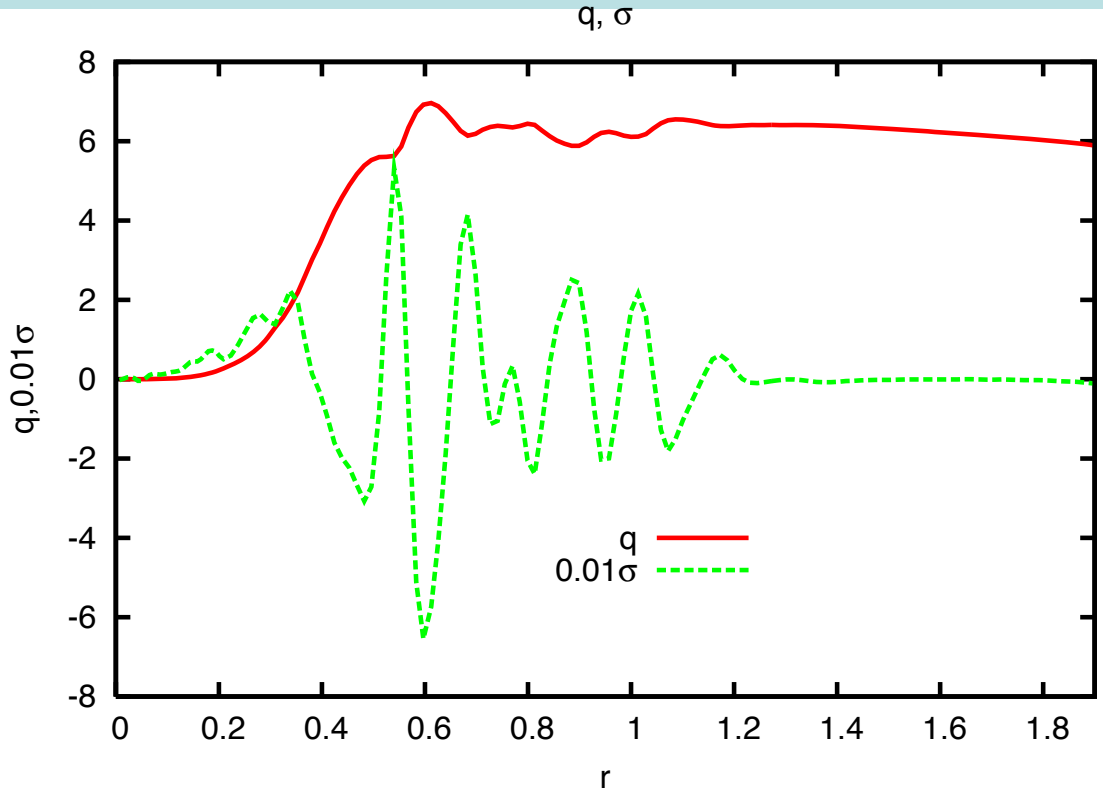

Kink stability criterion for previous case is consistent turbulence in simulation. The turbulence is external to stagnation region, so it may be benign

Conclusions

- theory of effect of axial magnetic field on Z pinch Rayleigh Taylor and kink stability
  - Rayleigh Taylor stable for moderate axial field
  - Kink mode easily destabilized
- Simulations in qualitative agreeement with theory
  - Rayleigh Taylor unstable for small axial field
  - Kink unstable, becomes turbulent, but outside the stagnation region
- Experiment
  - To be done at WIS
  - Compare with these results